RE-602

SPAR VI TECHNICAL REPORT FOR EXPERIMENT 76-22 - DIRECTIONAL SOLIDIFICATION OF MAGNETIC COMPOSITES

July 1980

Grumman Research Department Report RE- 602

SPAR VI TECHNICAL REPORT FOR EXPERIMENT 76-22 - DIRECTIONAL SOLIDIFICATION OF MAGNETIC COMPOSITES

by

Ron G. Pirich and David J. Larson, Jr

Research Department
Grumman Aerospace Corporation
Bethpage, New York 11714

Post-Flight Technical Report on Contract NAS 8-32219

for

George C. Marshall Space Flight Center
National Aeronautics and Space Administration
Marshall Space Flight Center, Alabama 35812

July 1980

Approved by:

Richard A. Scheuing
Director of Research

ABSTRACT

Three samples of eutectic Bi/MnBi were directionally solidified during a low-$\bar{g}$ interval (10^{-4} $\bar{g}$) aboard the SPAR VI flight. Comparison samples were solidified in a 1-$\bar{g}$ environment under identical furnace velocity and thermal conditions. In addition, eutectic Bi/MnBi composites were plane-front directionally solidified in 1-$\bar{g}$ over a range of growth velocities, thermal gradients, and solidification orientations with respect to the gravity vector. The Bi/MnBi eutectic was chosen for this investigation because its microstructure is characterized by a regular rod eutectic whose morphology may be sensitive to thermo-solutal convection and because one of its components, MnBi, is ferromagnetic. Therefore, the magnetic properties can be used to provide an efficient and sensitive measurement of the effect of convection on solidification processing.

Morphological analyses on samples that were directionally solidified during the 240-s low-$\bar{g}$ interval of the SPAR VI flight experiment show statistically smaller interrod spacings and rod diameters with respect to samples grown under identical solidification furnace conditions, in the same apparatus, in 1-$\bar{g}$. The magnetic property measurements indicate that the flight samples contain $\sim$ 7 v/o less dispersed MnBi than similarly processed 1-$\bar{g}$ samples of the same starting composition. Convectively driven temperature fluctuations in the melt, which result in unsteady liquid-solid interface movement in 1-$\bar{g}$, are suggested to explain the morphological change between low-$\bar{g}$ and 1-$\bar{g}$ solidification. As a result of these fluctuations, an adjustment between the interrod spacing, growth velocity, and total undercooling at the solidification interface is proposed to account for the observed change in volume fraction of dispersed MnBi.

Morphological analyses on samples grown in 1-$\bar{g}$ indicate little difference between results for different growth orientations with respect to the gravity vector, i.e., growth up (antiparallel), down (parallel) and horizontal (perpendicular). The magnetic properties are significantly affected, however, by the presence of a nonequilibrium magnetic phase. The amount of this phase is a sensitive function of the growth velocity, thermal gradient, and gravity vector orientation. The nonequilibrium phase transforms to the equilibrium ferromagnetic phase during isothermal heat treatment.

CONTENTS

INTRODUCTION

To assess the role of convection and coupled convective-diffusive transport on the crystal growth of eutectic alloys, the plane-front solidification of eutectic Bi/MnBi was investigated during both low-$\bar{g}$ and 1-$\bar{g}$ experiments. The Bi/MnBi eutectic was chosen because its microstructure is characterized by a regular rod eutectic morphology when grown by plane-front solidification with cooperative growth. One of the phases, MnBi, appears faceted while the other, Bi terminal solid solution, may be unfaceted. Therefore, the soldification of Bi/MnBi represents a candidate system thay may be sensitive to thermal and solutal instabilities produced by convective flows. In addition, the equilibrium MnBi phase is highly ferromagnetic and its magnetic properties can be used to characterize the effect of solidification processing and convection on rod size, shape, and alignment.

Since about 1960, considerable study has focused on the plane-front solidification of eutectic alloys (Ref 1), and more recently on thermo-solutal convection (Ref 2 and 3) that occurs when the fluid density depends on variables such as temperature and solute concentration. Theoretically, free convection might cause, for example, fluctuations in the rate of solidification (Ref 4), which would lead to microstructural variations along the growth direction. In a rodlike eutectic, these variations could lead to changes in volume fraction, rod diameter, interrod spacing, and electronic properties, e.g., magnetic properties, associated with these microstructural characteristics.

In the high furnace rate and thermal gradient regime of $V \sim 30$ cm/h and $G_L \sim 100°C/cm$, the mass transfer film thickness, δ_m, is expected to be on the order of 50 μm in 1-$\bar{g}$ and 500 μm in a 10^{-4} $\bar{g}$ environment, while the solute boundary layer, or Stefan length, p^{-1}, is on the order of 25 μm for V = 30 cm/h for eutectic Bi/MnBi (Ref 5). The ratio δ_m/p^{-1} or $p\,\delta_m$ is, therefore, ~ 2 in 1-$\bar{g}$ and ~ 20 in 10^{-4} $\bar{g}$ suggesting a possible convective interaction in 1-$\bar{g}$ even at this high growth velocity and near diffusion control in 10^{-4} $\bar{g}$ environment.

Samples were grown up, down, and horizontal to the gravity field in an effort to change the degree of thermal and solutal convection present. Ground base

experiments ($1\text{-}\bar{g}$), were performed over a range of furnace velocities, V, $0.5 \leq V \leq 50$ cm/h, and thermal gradients in the liquid at the solidification interface, G_L, $20 \leq G_L \leq 150$°C/cm. Therefore, $p\,\delta_m$, $0.2 \leq p\,\delta_m \leq 3.5$. For example, a statically stable fluid (net fluid density < 0) might be expected for eutectic Bi/MnBi in a growth up configuration with sufficiently large temperature gradient since the fluid density of Mn is less than Bi, thereby minimizing convective effects in the absence of sufficiently large radial temperature gradients near the solidification interface. Similarly, convective flow should be maximum when the growth is horizontal because both thermal and solutal convection are present. However, definitive analytic analysis or experimental evidence for a priori prediction of the effects of these levels of $p\,\delta_m$ on microstructure and associated electronic properties of directionally solidified eutectics have not yet been developed or determined. The objective of this investigation was, therefore, twofold:

(1) Determine the effect of a reduction in gravity for samples grown in the same apparatus under identical furnace conditions except for the suppression of the magnitude of the gravitational force; and

(2) Attempt to alter the degree of thermosolutal convection in $1\text{-}\bar{g}$ by changing the solidification direction with respect to the gravity vector over a range of V, G_L and, therefore, $p\,\delta_m$.

EXPERIMENTAL PROCEDURE

SAMPLE PREPARATION

Bi/MnBi samples were prepared using commercially pure Mn (99.9 w/o) and high purity Bi (99.999 w/o). Both were melted together in an evacuated ($\sim 10^{-5}$ torr) high purity quartz crucible (1.0-cm inner diameter) above 446°C, the temperature at which the stoichiometeic MnBi compound forms (Ref 6). The melt was electromagnetically stirred for a period of 16 h to ensure homogenization. The Bi-Mn phase diagram (see Fig. 1) was determined in the vicinity of the eutectic composition by means of differential scanning calorimetry and chemical spectrohotometric absorbance (Ref 7). The eutectic composition was found to be 0.72 $\pm$ 0.03 w/o Mn (2.69 $\pm$ 0.08 a/o Mn), which results in an MnBi volume fraction of 3.18 $\pm$ 0.09 v/o. Portions of these eutectic starting boules were then encapsulated in a specially designed, evacuated quartz ampoule (0.4-cm inner diameter), illustrated in Fig. 2. The eutectic Bi/MnBi sample was localized by means of tight-fitting, high purity graphite spacers and quartz wool "O" rings at the appropriate position for solidification. A melt back interface was used to minimize leak-by of the melt. The ampoules were instrumented with very fine chromel-alumel thermocouples (0.0015-in. bead diameter) sheathed in MgO insulation with a 0.010-in diameter 304 stainless steel outer tube. The preflight and postflight ground base experiments consisted of four ampoules: two directionally solidified growth up and instrumented with four equally spaced thermocouples, and two directionally solidified growth down and instrumented with one thermoucouple per ampoule. A similar arrangement was used for the flight experiment. Those samples investigated in other ground base experiments, i.e., grown at velocities and thermal gradients other than the SPAR VI flight conditions, were instrumented with one thermocouple. The presence of these thermocouples did not appear to perturb significantly the solidification processing either through chemical contamination or heat transfer. In fact, the thermal conductivity of the thermocouple probes was found to be very near the thermal conductivity of liquid eutectic Bi/MnBi.

DIRECTIONAL SOLIDIFICTAION PROCESSING

The preflight, flight, and postflight experiments were performed using the Bridgman-Stockbarger method in an automatic directional solidification system

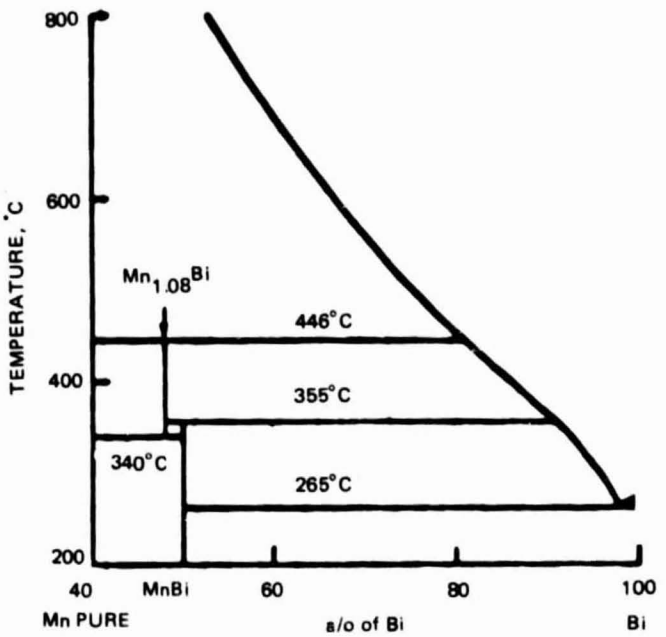

a) As Determined by Chen

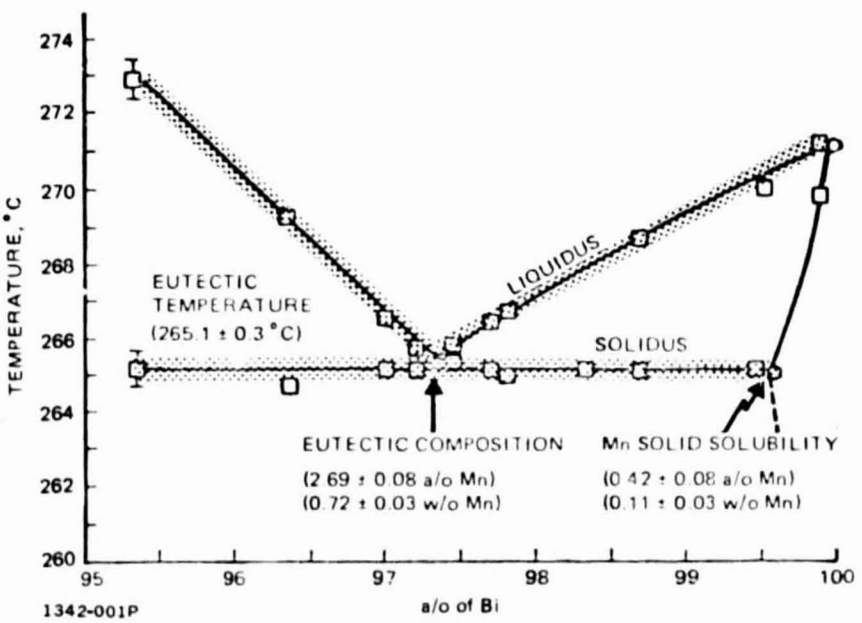

(b) In the Vicinity of Eutectic as Determined in This Work

Fig. 1 Bi-Mn Phase Diagram

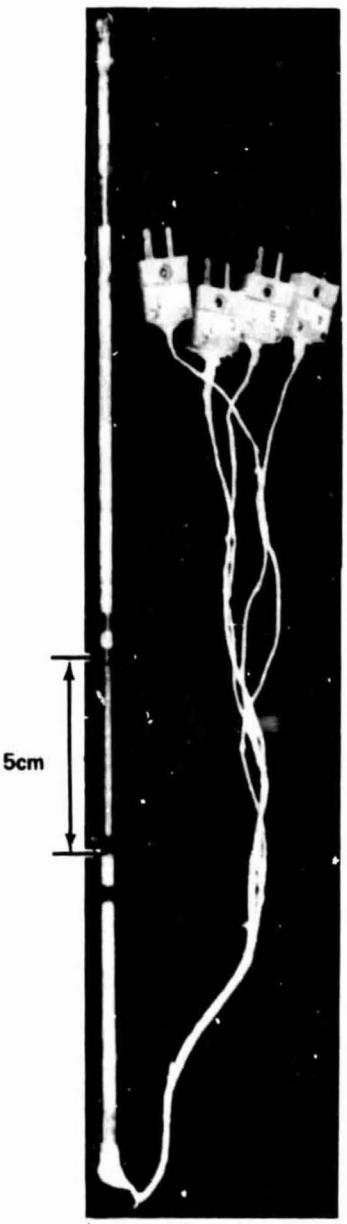

a) Actual Instrumented Ampoule Used for Solidification Processing

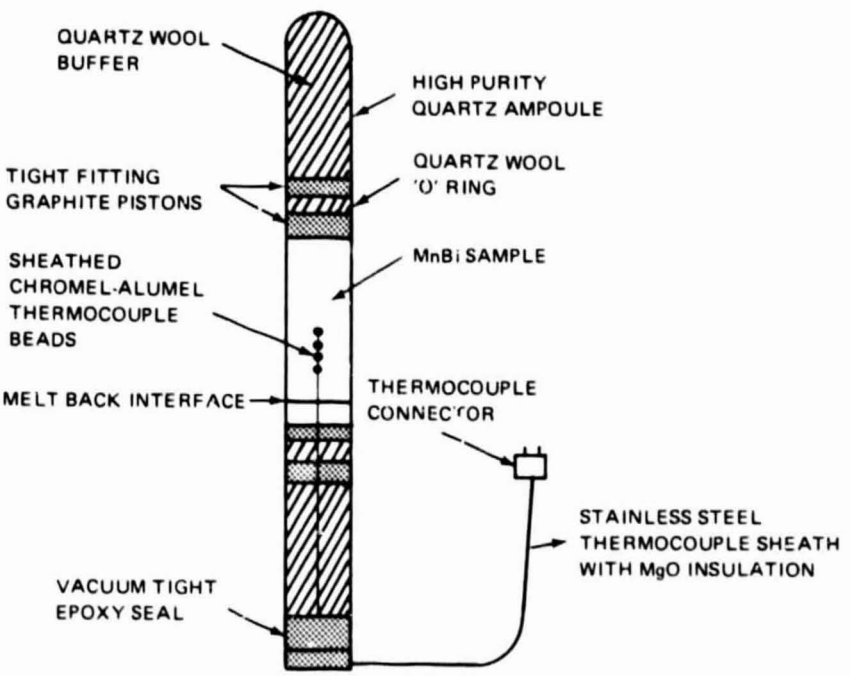

b) Representative Schematic

1342-002P
0868-007P

Fig. 2 Eutectic Bi/MnBi Ampoule Configuration

(ADSS) built by General Electric (Ref 8). The ADSS apparatus consists of four symmetrically mounted furnace assemblies, each completely independent with respect to temperature and linear velocity of movement. Schematics of the furnace assembly and actual apparatus are shown in Fig. 3 and 4, respectively. For the preflight, flight, and postflight experiments, each furnace produced about the same gradient (~100°C/cm) and moved at the same linear speed (~30 cm/h). In addition, furnaces mounted in opposition with respect to the assembly mounting plates moved in the same direction so that the total ADSS momentum was zero. The apparatus also underwent intrinsic vibrational testing so as to monitor the level of external force produced by furnace movement at the location of the ampoule. This level was found to be $< 10^{-5}$ $\bar{g}$. Each ADSS furnace assembly produced a well controlled unidirectional thermal gradient near the solidification temperature of eutectic Bi/MnBi at 265.1 $\pm$ 0.3°C. This gradient can be varied from 10°C/cm to 200°C/cm by adjusting the temperature of the furnace nichrome heating elements and the fluid cooled copper quench block. The linear furnace velocity can be varied from 0.1 to 100 cm/h. A similar furnace unit was used for the other ground base investigations.

PREFLIGHT, FLIGHT, & POSTFLIGHT EXPERIMENTS

Two preflight experiments were conducted in the ADSS apparatus at Marshall Space Flight Center in accordance with the SPAR VI flight operational timeline. One of these tests - the Pre-Installation Acceptance Test (PIAT) - was conducted with the ADSS unit separated from the other flight experiments, in ambient atmosphere and temperature, and in a vertical geometry (growth up and down). The purpose of the PIAT was to ensure that plane-front solidification occurred at the SPAR VI solidification conditions, and to establish baseline criteria for the flight experiment. In the other preflight experiment (All-Systems Test), the entire apparatus was placed in a sealed cannister filled with dry N_2 gas and run in conjunction with the other flight experiments. All conditions were identical with the flight experiment except for the presence of the vertical gravity vector. The All-Systems Test provided 1-$\bar{g}$ samples to be used for direct comparison with the SPAR VI flight samples.

The SPAR VI flight experiment began with initiation of furnace heating 90 min before launch. At 5 min before launch, each in situ sample thermocouple temperature was monitored and compared against the baseline criteria established

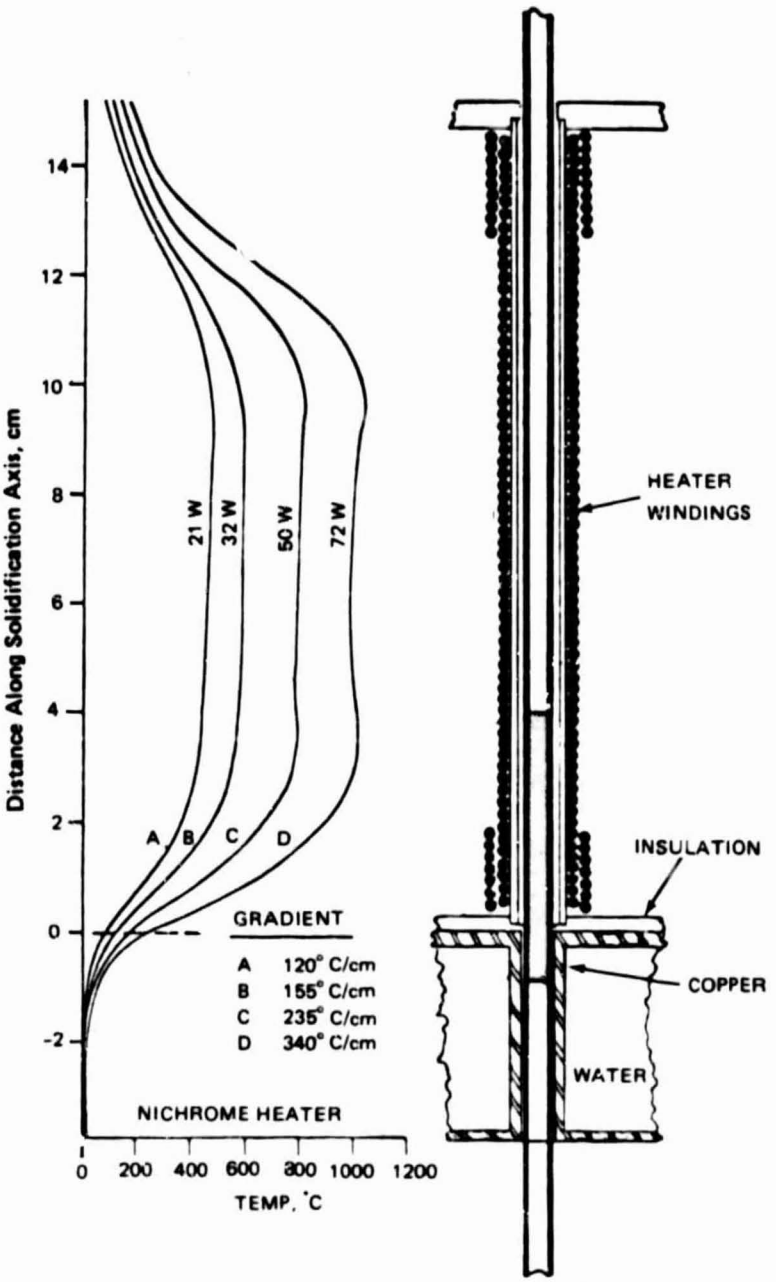

Fig. 3 Schematic Representation of ADSS Furnace Assembly and Representative Thermal Profiles

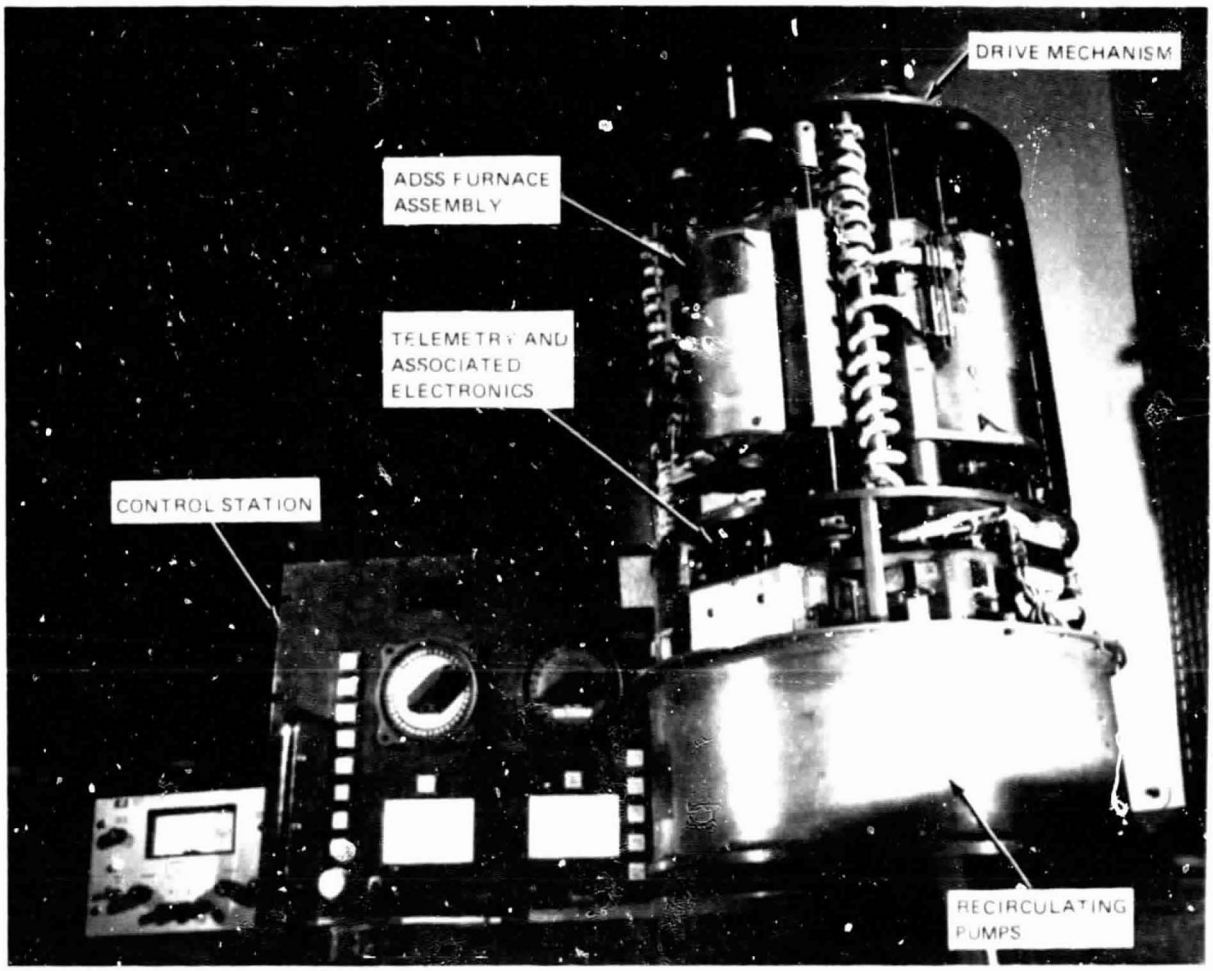

1342-604P

Fig. 4 Actual ADSS Flight Apparatus With Ground Base Control Station

following the PIAT test. After launch, directional solidification commenced ~15 s after low-$\bar{g}$ had been attained or ~120 s after launch. Directional solidification proceeded through the low-$\bar{g}$ interval (~240 s) and continued even after deployment of the drop parachute, terminating ~728 s after launch. By this time, the entire length of each Bi/MnBi sample (~5 cm) had been directionally solidified with ~1.8 cm plane-front directionally solidified in low $\bar{g}$.

A PIAT type test was also conducted after the flight experiment to ensure that no systematic apparatus anomalies had occurred as a result of the launch.

FLIGHT (Low-$\bar{g}$) & ALL-SYSTEMS TEST (1-$\bar{g}$) COMPARISON

Each SPAR VI flight (low-$\bar{g}$) and All-Systems Test (1-$\bar{g}$) sample was partitioned, as shown in Fig. 5, at the axis of solidification as well as at three fraction solidified locations by means of a diamond impregnated string saw. The string saw was used to avoid unnecessary stress during the sectioning process.

The top half (containing no thermocouple remanant) of each axial section was used for both magnetic and morphological analysis. The remaining half was used only for morphological study. Comparison between flight and ground base samples was made at the same fraction solidified or fraction solidified interval for samples grown in the identical furnace assembly so as not to skew the results systematically. All comparisons were made in the low-$\bar{g}$ interval of solidification.

GROUND BASE (1-$\bar{g}$) MATRIX EXPERIMENT

In a series of ground base investigations, samples were grown parallel, antiparallel, and perpendicular to the gravity field at growth velocities between V = 3 and 30 cm/h and thermal gradients, G_L = 20 and 150°C/cm. The hot zone was adjusted, regardless of growth orientation with respect to the gravity field, to maintain a constant thermal gradient in the liquid in both the high and low thermal gradient regimes. One transverse fraction solidified location, near the thermocouple bead, was used for morphological study. Several longitudinal locations were observed to ensure that cooperative growth had occurred as a function of fraction solidified. In addition, two fraction solidified sections per growth condition were used for magnetic property analysis. For two ampoules, the

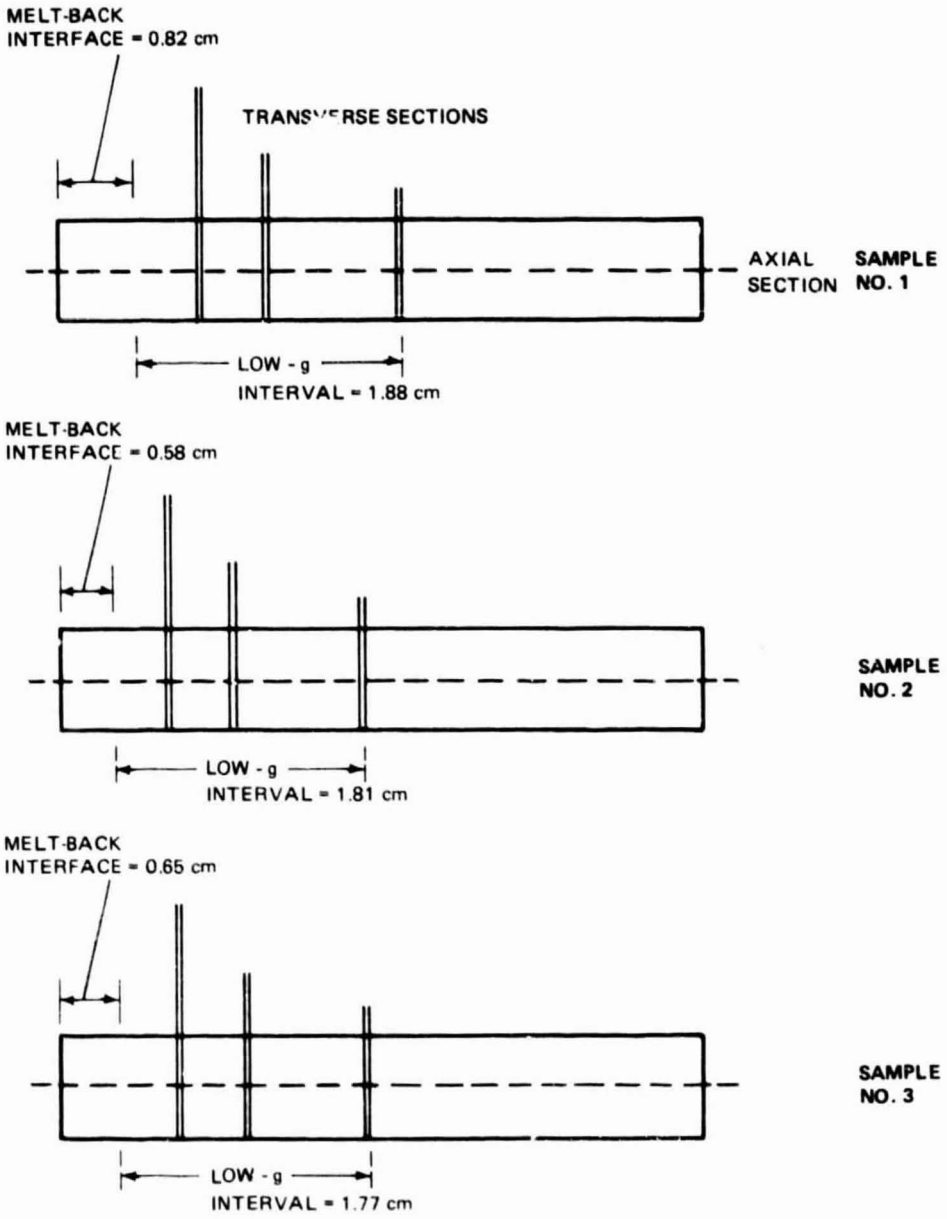

Fig. 5 Schematic Representation of Sample Partitioning of All Systems Test and Flight Experiment Samples

entire length was equipartitioned and the magnetic properties determined as a function of fraction solidified.

MICROSTRUCTURAL, THERMAL, & MAGNETIC PROPERTY ANALYSIS

Sample morphology (dispersed MnBi rod size, volume fraction, and rod alignment) was determined from optical micrographs of mechanically polished surfaces both parallel and perpendicular to the solidification direction. Fifteen micrographs of a mechanically polished surface at each tranverse fraction solidified location were analyzed as to MnBi rod area, interrod spacing, and volume fraction. Analysis was performed using a computer aided Leitz particle analyzer system.

For the preflight and flight experiment, each in situ thermocouple, four furnace control thermocouples, and two reference thermistors were monitored at about one reading per second for each furnace assembly. These measurements were transmitted via telemetry and recorded both in digital and analog format. The subsequent analog voltages were converted to temperature in degrees centigrade by assuming a quadratic relationship between voltage and temperature. Due to the lack of point to point grounding in the ADSS apparatus, resolution of the in situ thermocouple measurements was limited to $\pm$ 0.08 mV($\pm$2.0°C). For the remaining ground base testing, in situ thermocouple measurements were monitored using a Digitec Thermocouple acquisition system with a temperature resolution of $\pm$0.2°C.

Magnetic properties were determined from magnetization measurements of cylindrically shaped samples. Magnetization was measured parallel and perpendicular to the solidification direction at 290,77, and 4.2 K in applied fields up to 230 kOe at the Francis Bitter National Magnet Laboratory, using a low frequency vibrating sample magnetometer. A Princeton Applied Research high frequency vibrating sample magnetometer was used at Grumman to measure magnetization as a function of angle with respect to solidification direction, applied field up to 17 kOe over a temperature from 290 K to the eutectic melting temperature of 538 K. A portion of the magnetic characterization facility used at Grumman is shown in Figure 6.

It had been anticipated that because the equilibrium MnBi phase is ferromagnetic at and below room temperature, its magnetic properties could be used to measure the effect of particle morphology (e.g., average rod size and particle alignment) and the effect of solidification processing and convection on the

1342-006P

Fig. 6 Part of Magnetic Characterization Facility at Grumman

morphology. For example, the intrinsic coercivity, ${}_mH_c$, of ferromagnetic materials should increase with decreasing particle size and approach the theoretical maximum when the particle contains only one magnetic domain (single domain behavior). It was observed, however, that plane-front directionally solidified eutectic Bi/MnBi with comparable morphologies differed dramatically in magnetic properties depending on solidification processing conditions and heat treatment after solidification (Ref 9-12). As is seen in Fig. 7, the room temperature (300 K) intrinsic coercivity for samples processed only by directional solidification (as-grown state) appears to be a weakly dependent function of the average dispersed MnBi particle size except for higher growth velocities where the samples become almost paramagnetic in character. This behavior is supported by the decrease in remanent magnetization shown by samples in the as-grown state. For the same samples sufficiently heat treated (at 250°C for periods greater than 24 h), a dramatic increase is observed not only in room temperature remanent magnetization but also in intrinsic coercivity. Another magnetic phase, other than the expected equilibrium (so-called LTP) MnBi, which occurs in directionally-solidified material, has been identified as the origin of these differences. This new magnetic phase, termed the high coercivity or HC phase, is found to coexist with the LTP phase. The HC phase is paramagnetic at room temperature and orders ferrimagnetically (Ref 10) near 250 K with an intrinsic coercivity $\sim$110 kOe at 77 K, measured parallel to the solidification direction. With the applied field parallel to the solidification direction, the hysteresis curves corresponding to the LTP and HC phases are distinct and separate both at room temperature and 77 K (Fig. 8) so that determining the amount of each phase present is straightforward (Ref 9-13). The magnetization can be measured with an uncertainty of $\pm 10^{-3}$ emu. Since eutectic samples used for magnetization studies have moments between $\sim$0.75 emu for 100% HC phase and $\sim$1.70 emu for 100% LTP phase, for an applied field of 150 kOe at room temperature, the uncertainty in determining the amount of each magnetic phase (and the volume fraction of MnBi) varies from $\pm$ 0.3 % for 100% LTP phase to $\pm$ 1.0% for a 30/70% combination of LTP/HC phases at the eutectic Bi/MnBi composition.

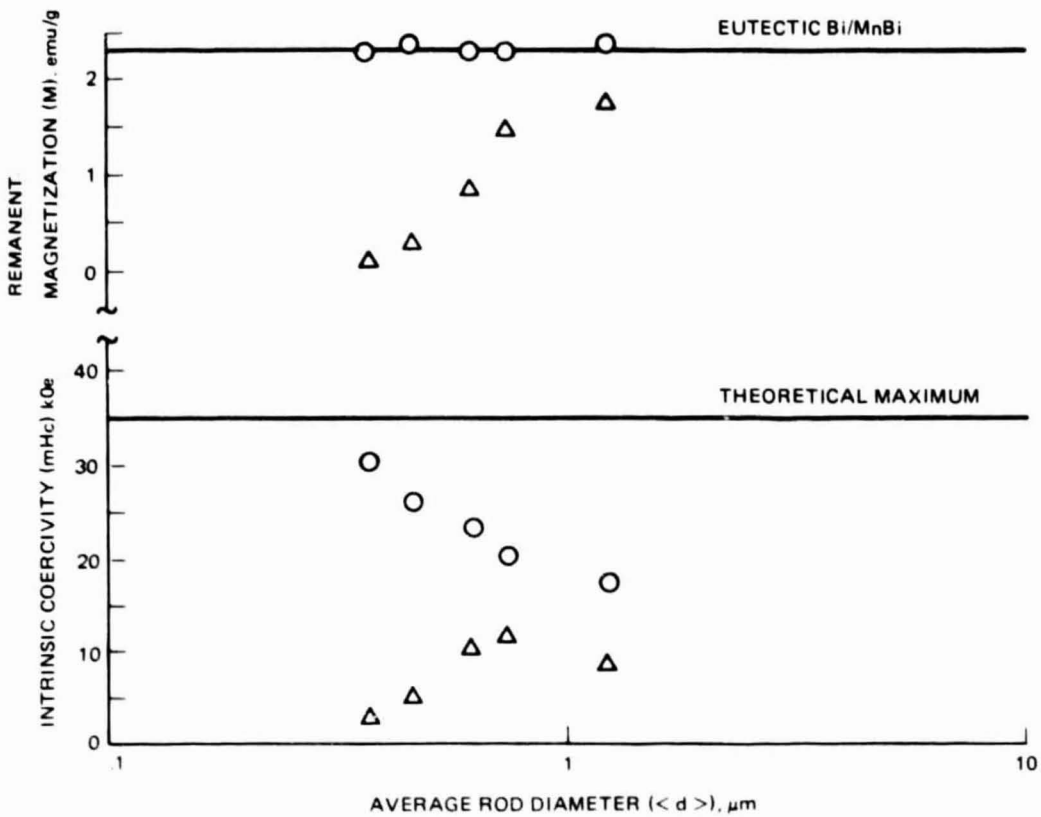

1342-007P

Fig. 7 Dependence of Room Temperature Remanent Magnetization and Intrinsic Coercivity on Mean MnBi Rod Diameter in As-Grown (Δ) and Heat-Treated States (o)

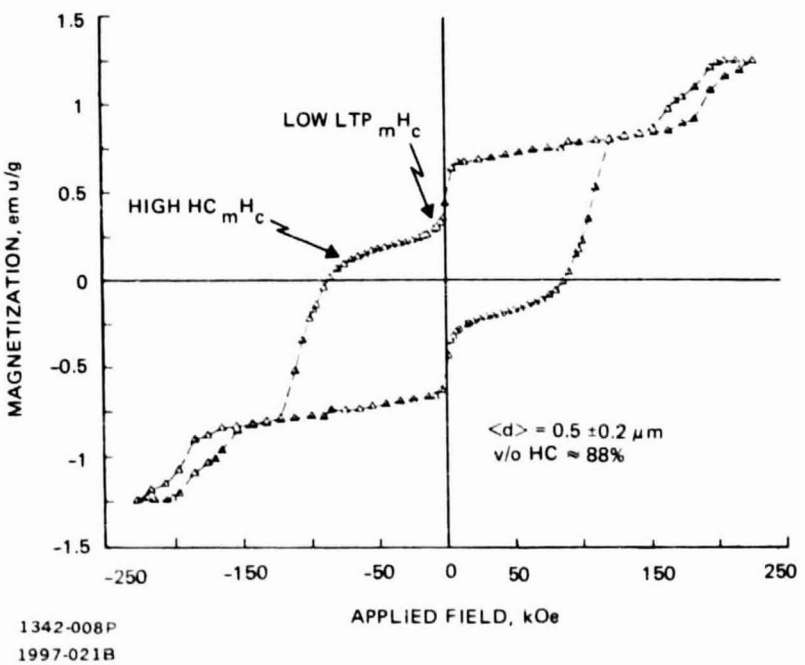

Fig. 8 Hysteresis Curve Measured Parallel to the Solidification Direction at 77 K for Sample Containing Combinations of HC and LTP MnBi Phases

RESULTS

LOW-$\bar{g}$ EXPERIMENT - GENERAL OBSERVATIONS

On October 17, 1979, SPAR VI was flown successfully. The flight ampoules were removed the same day, and were returned to Grumman on October 19. As shown in Fig. 9, ampoule No. 1 and 3 were completely intact; their in situ themocouples (four in each ampoule) were still functioning properly. Ampoule No. 2 had been broken near the top retaining washer of the ADSS furnace No. 2 assembly, but the fracture was located sufficiently far away from the Bi/MnBi sample so that the sample was not affected. Fracture most probably occurred at impact, i.e., after the sample had completely solidified. This probability is supported by the recovery team which reported a large gash in the outer payload skin near the 76-22 apparatus (see Fig. 10), apparently caused by the payload being dragged over rough terrain at the impact site. Ampoule No. 2 was singly instrumented, and its thermocouple was also still functioning properly. Ampoule No. 4, also singly instrumented, was broken at launch. This is confirmed by a sudden disturbance in thermocouple output as observed from the telemetry data at launch. Ampoule breakage may have been caused by the rather severe vibration of the rocket bumping against the gantry. Fortunately, the molten Bi-Mn quickly quenched on the lower ADSS base plate and did not interfere with any other furnace assembly.

Evaluation of the telemetry data indicates that all in situ and furnace thermocouples, reference transistors, and furnace assemblies operated properly. The telemetry data also indicate that one of the recirculating pumps malfunctioned, but because of the large thermal mass of each furnace, and since the ADSS has two such pumps, no noticeable effect on the temperature of the fluid cooled furnace assembly quench blocks was discernable.

Several x-ray radiographs and macrophotographs of the ampoules were taken, as shown in Fig. 11 and 12. They indicated no unusual porosity except for ampoule No. 2 in which the volume made available by a slight leak-by of molten Bi-Mn at launch (furnace was above quench block) caused separation of the sample into four distinct parts. This did not have any adverse effects on evaluation of sample thermal data since the first separation occurred below the termination of the in situ thermocouple and after solidification during the low-$\bar{g}$ interval.

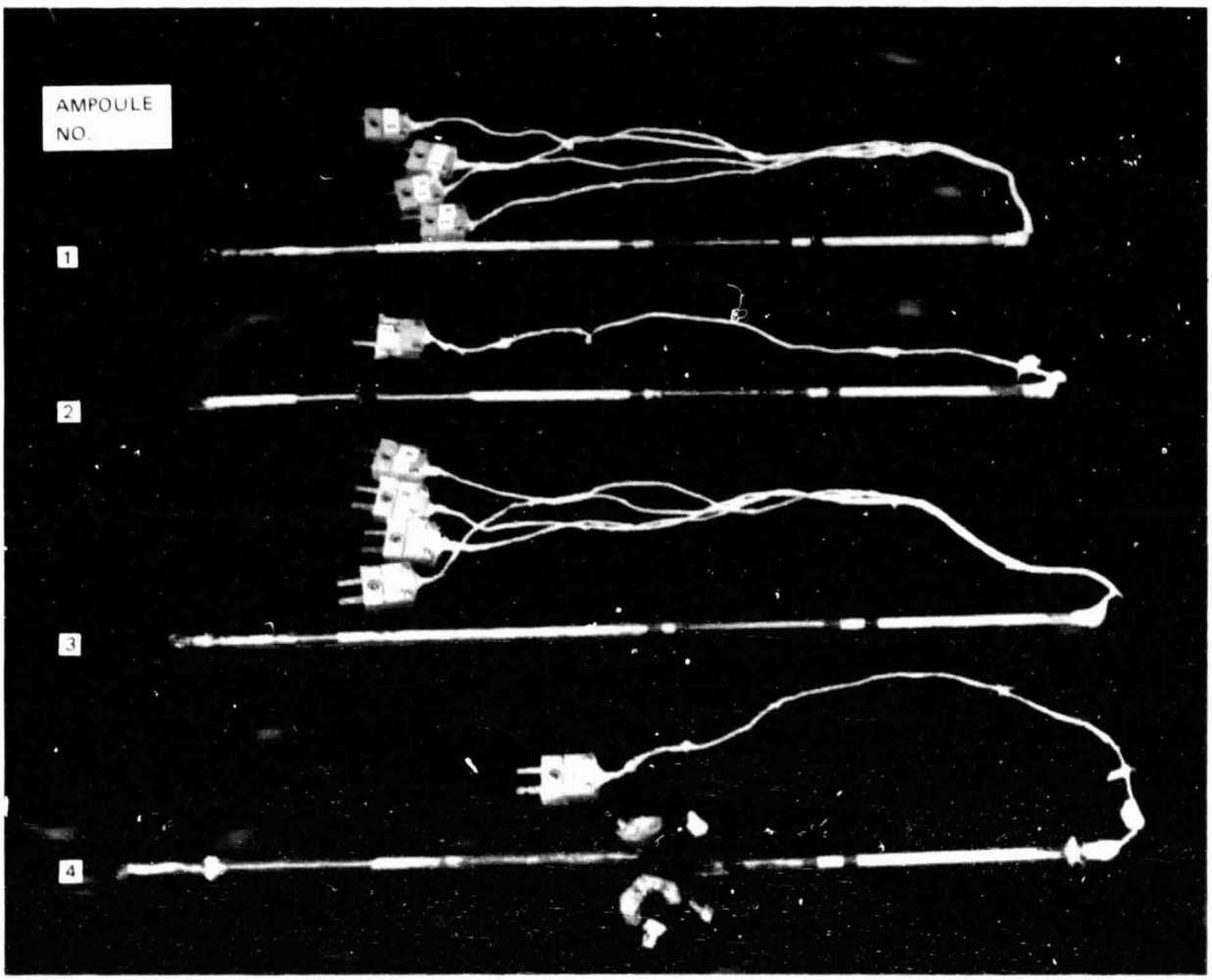

1342-009P

Fig. 9 SPAR VI Flight Ampoules as Received After the Flight Experiment

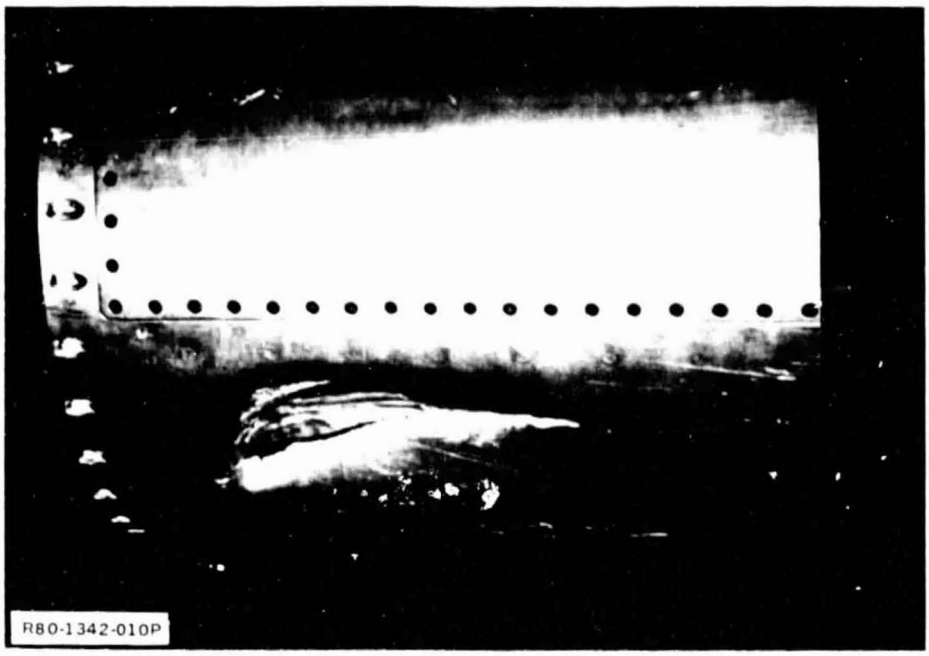

Fig. 10 Photograph After SPAR VI Flight Showing Gash in Outer Payload Skin Near the 76-22 Apparatus

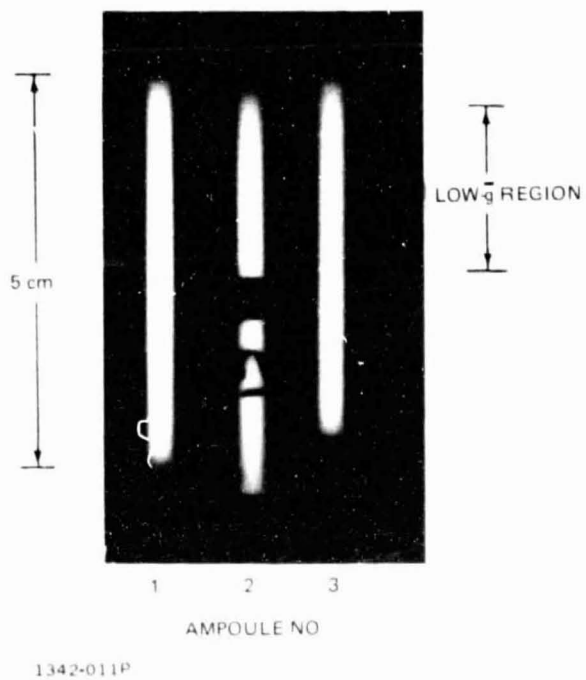

Fig. 11 X-Ray Radiograph of Flight Ampoules No. 1, 2 & 3 After SPAR VI Flight

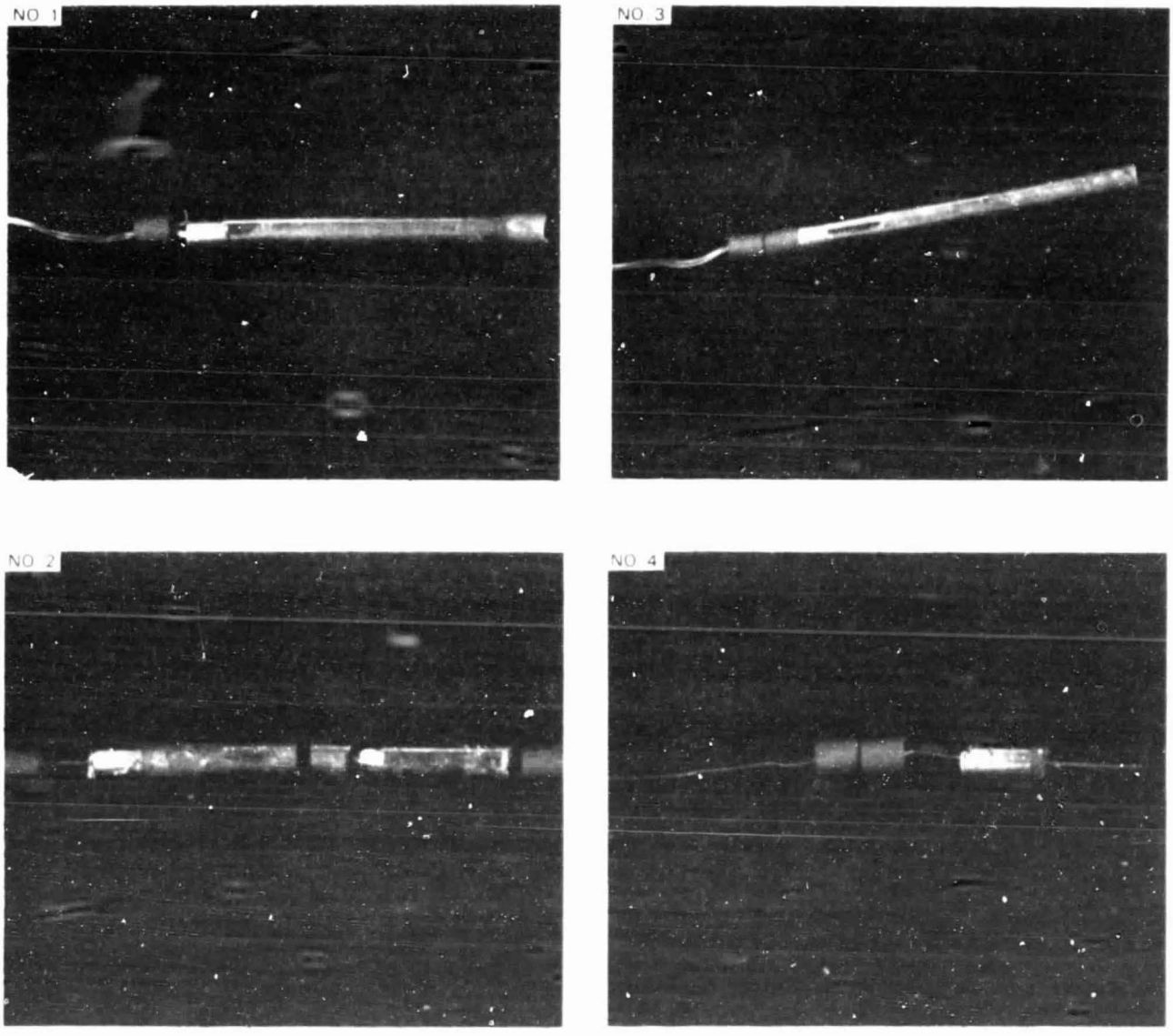

1342-01CP

Fig. 12 Photographs of Flight Samples After Removal From Ampoules

FLIGHT (Low-$\bar{g}$) AND ALL-SYSTEMS TEST (One-$\bar{g}$) COMPARISON

Morphology

Plane-front solidification with cooperative growth of eutectic Bi/MnBi results in an aligned ensemble of MnBi rods, with length to diameter ratios on the order of 100, dispersed in a Bi-terminal solution matrix on the order of 0.1 w/o Mn. Typical Transverse and longitudinal microstructures are shown in Fig 11. The long axis of the rods is parallel to the solidification direction. The morphology of the rod cross-sections is degenerate-faceted and chevron-shaped at the lower furnace velocities ($V < 3.0$ cm/h) as shown in Fig 13, and more circular-like at higher furnace velocities ($V > 20$ cm/h) as shown in Fig. 14. Mean rod diameters $\langle d \rangle$, and interrod spacings, $\langle \lambda \rangle$, as determined by fitting the measured rod diameter and interrod spacing distributions with a Poisson distribution function and minimizing the x^2, were found to vary in the expected manner (Ref 1) with growth velocity, V, i.e.,

$$\langle d \rangle, \langle \lambda \rangle \sim V^{-1/2} \qquad (1)$$

Very uniform, cooperative growth was observed from the beginning of solidification, through the low-$\bar{g}$ interval until the deployment of the SPAR VI flight parachute (Fig. 15). The deployment of the parachute resulted in a large perturbation to the solidification processing with an abrupt termination of cooperative growth see Fig. 16, and in a melting back of the solidification interface as determined by the in situ thermocouple data.

Morphological measurements of MnBi rod diameter and interrod spacing distributions on all three flight samples solidified during the low-$\bar{g}$ interval show a statistically significant difference with respect to the same fraction solidified regions of samples grown under identical furnace conditions, in the same furnace assembly, in 1-$\bar{g}$ (as seen in Table 1). This is shown in Fig. 17 for samples grown in furnace assembly No. 1. Both the MnBi rod diameter and interrod spacing distributions have smaller values for the low-$\bar{g}$ grown samples, with mean rod diameters and mean interrod spacings 30 $\pm$ 9% and 35 $\pm$ 12% smaller, respectively (Fig. 18 and Table 1). This behavior was similar at each fraction-solidified location measured and for each sample solidified. The measured MnBi volume fraction of the flight samples (2.96 $\pm$ 0.38 v/o), as determined from quantitative morphological analysis, was statistically equivalent to the All-Systems Test

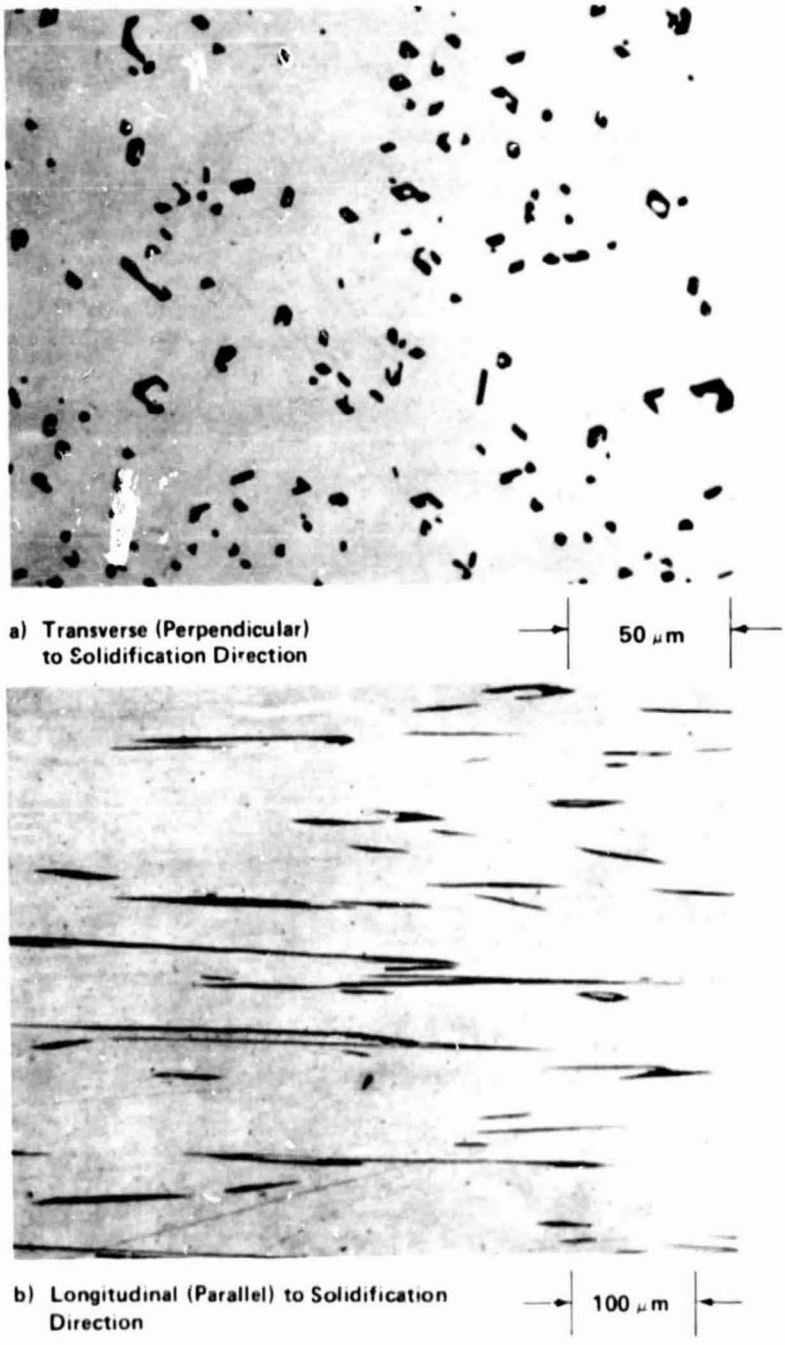

Fig. 13 Eutectic Bi/MnBi Cooperative Growth Morphology at V = 0.8 cm/h and G_L = 150° C/cm

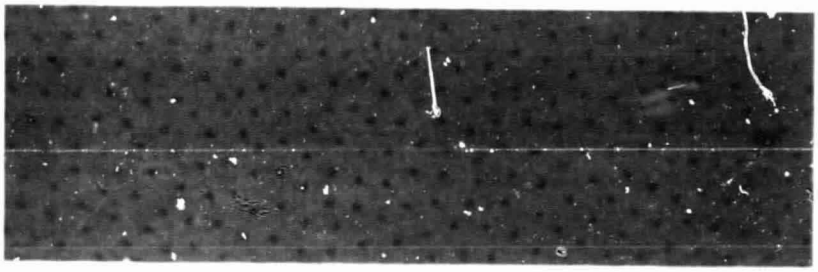

a) Transverse (Perpendicular) to Solidification Direction — 5 μm

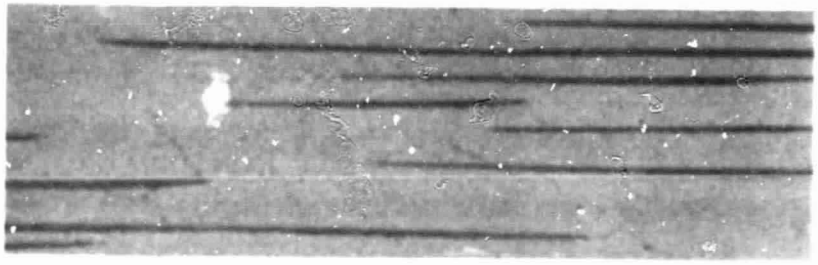

b) Longitudinal (Parallel) to Solidification Direction — 5 μm

134240141

Fig. 14 Eutectic Bi/MnBi Morphology Produced by Plane Front Solidification with Cooperative Growth at V = 30 cm/h, G_L = 100 C/cm Grown up with Respect to Gravity Vector

1342-015P

Fig. 15 SPAR VI Flight Sample No. 1 Morphology in Low-$\bar{g}$ Interval Longitudinal (Parallel) to Solidification Direction

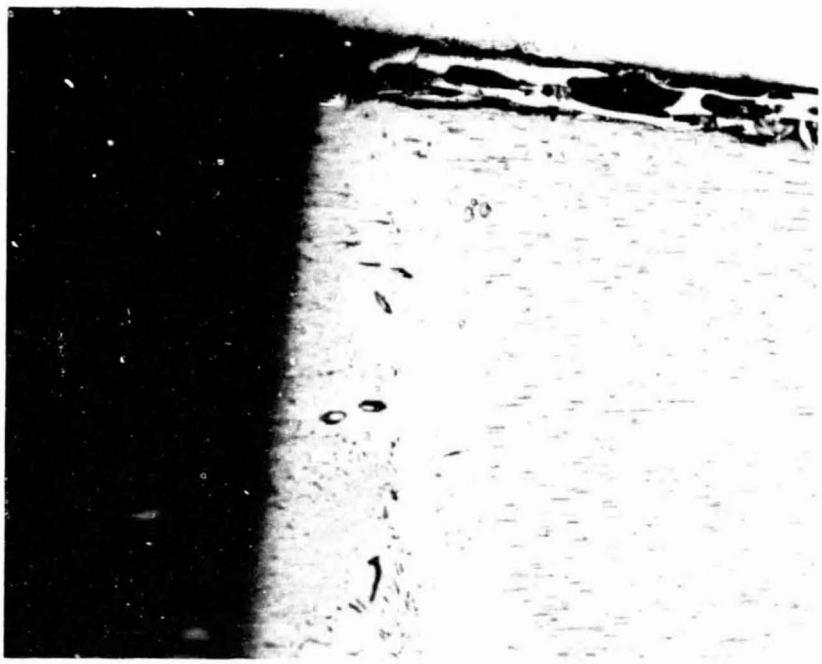

1342-016P

Fig. 16 Microstructure of Flight Sample No. 2 Longitudinal (Parallel) to Solidification Direction Near Region of First Separation. This region corresponds to deployment of drop parachute.

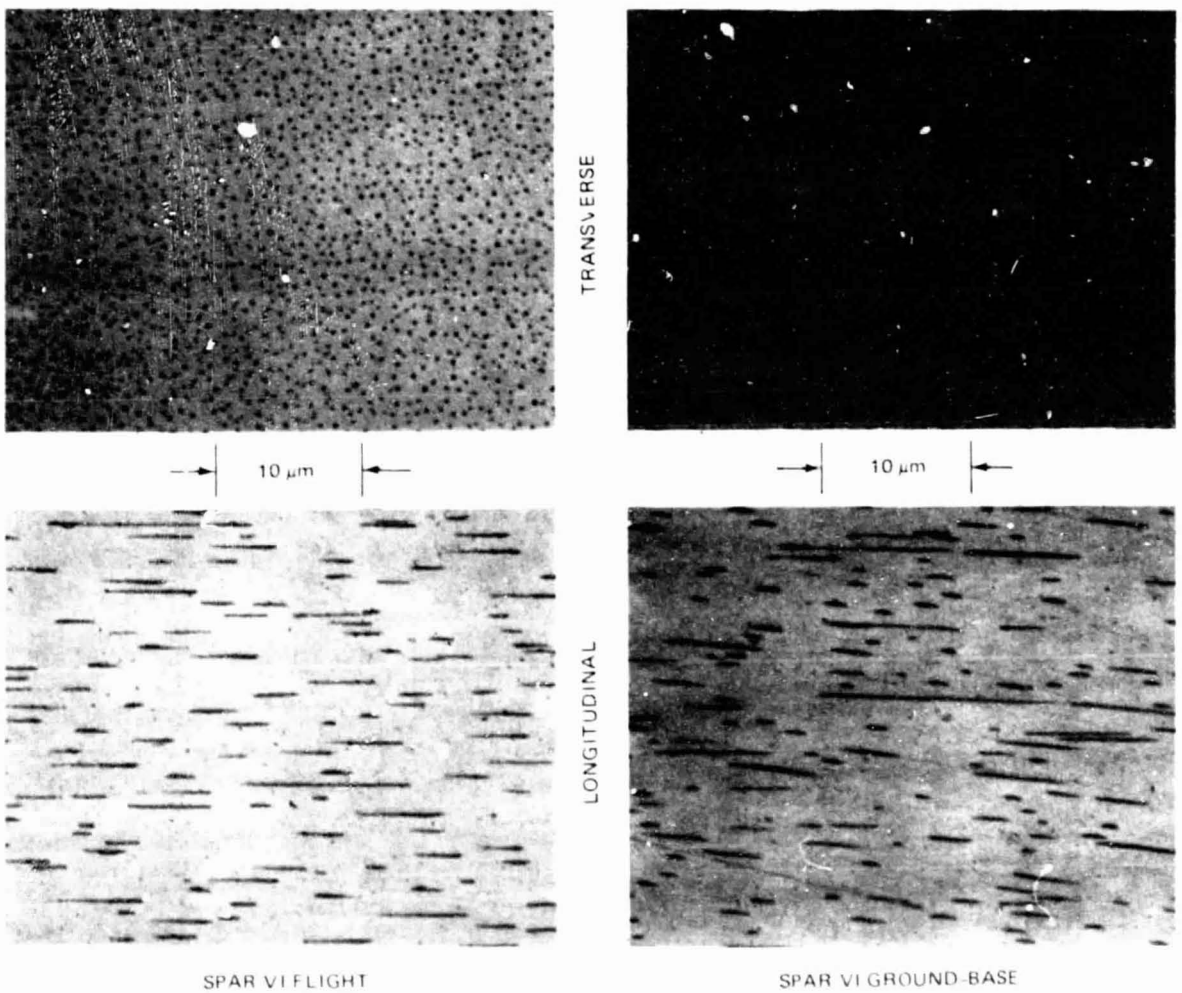

1342-017P

Fig. 17 Comparison of Flight and All-Systems Test Microstructures for Samples Processed in Furnace Assembly No. 1 at Same Fraction Solidified Location During Corresponding Interval of Low-$\bar{g}$ Solidification

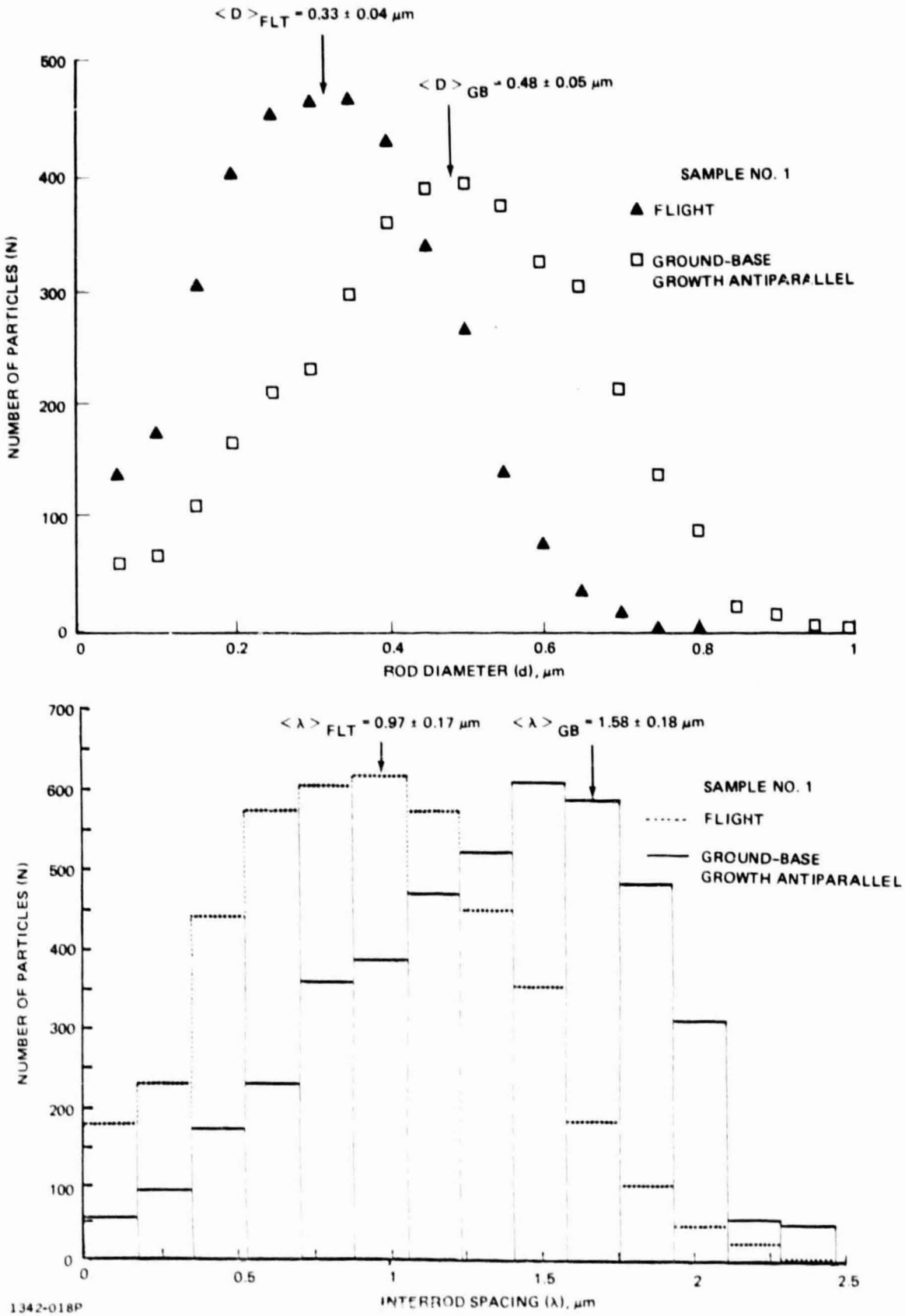

Fig. 18 Comparison of All-Systems Test & Flight MnBi Rod Diameter & Interrod Spacing Distributions for Samples Grown in Furnace Assembly No. 1 Including Statistics From All Transverse, Low-$\bar{g}$ Sections

Table 1 Comparison of Thermal, Morphological, & Magnetic Properties for Samples Grown During All-Systems Test 1-$\bar{g}$ & SPAR VI Flight (Low-$\bar{g}$) in Identical Furnace Assembly Apparatus. Comparison is Normalized to Low-$\bar{g}$ Regions of Solidification.

EXPERIMENTAL MEASUREMENT	All-Systems Test (1-$\bar{g}$) Furnace Assembly No.			SPAR VI Flight (10^{-4} $\bar{g}$) Furnace Assembly No.		
	1	2	3	1	2	3
Bulk starting composition, (w/o Mn)	0.71 ±0.03	0.72 ±0.03	0.72 ±0.03	0.72 ±0.03	0.71 ±0.03	0.72 ±0.03
Furnace assembly velocity, x 10^{-3} cm/s	8.0 ±0.6	7.8 ±0.3	7.7 ±0.3	7.8 ±0.5	7.5 ±0.3	7.3 ±0.3
Furnace hot zone temperature, °C	451 ± 5	462 ± 5	451 ± 5	446 ± 5	460 ± 5	446 ± 5
Furnace quench block temperature, °C	48.5 ± 1.2	47.5 ± 1.2	48.5 ± 1.2	48.0 ± 1.2	48.0 ± 1.2	48.0 ± 1.2
Solidification temperature, °C	265.3 ± 2.0	...	265.1 ± 2.0	262.4 ± 2.0	...	262.6 ± 2.0
Thermal gradient at interface/liquid, °C/cm	102.6 ± 8.6	...	108.1 ± 8.8	105.1 ± 6.7	...	107.8 ± 6.9
Thermal gradient at interface/solid, °C/cm	179.9 ±15.0	...	177.1 ±14.3	162.5 ±10.4	...	173.4 ±11.7
Mean MnBi interrod spacing (λ), μm	1.58 ±0.18	1.60 ±0.19	1.43 ±0.19	0.97 ±0.17	0.98 ±0.17	1.05 ±0.16
Mean MnBi rod diameter (D), μm	0.48 ±0.05	0.46 ±0.05	0.48 ±0.05	0.33 ±0.04	0.32 ±0.04	0.35 ±0.04
Volume percent HC MnBi phase normalized to v/o MnBi, %	95.3 ± 0.1	95.1 ± 0.1	95.2 ± 0.1	95.3 ± 0.1	95.2 ± 0.1	95.3 ± 0.1
Volume percent MnBi from magnetic property measurements, %	3.18 ±0.03	3.16 ±0.03	3.19 ±0.03	2.96 ±0.03	2.93 ±0.03	2.98 ±0.03
Resistance to demagnetization (intrinsic coercivity) for partially annealed 50% equilibrium/nonequilibrium MnBi magnetic phases, kOe	25.6 ± 0.5	...	...	30.0 ± 0.5	...	...

R80-1342-038P

samples (3.18 ± 0.47 v/o). The local inhomogenity in volume fraction noted in ground base samples was also present in the flight samples and tended to increase significantly the width of volume fraction distributions observed by morphological measurements.

Thermal Properties

Comparison of thermal data through the solidification temperature was limited to samples in furnace assemblies No. 1 and No. 3 (each sample instrumented with four in situ thermocouples) since these samples had at least one thermocouple terminate within the low-$\bar{g}$ fraction solidified region. The sample in furnace assembly No. 2 was instrumented with only one thermocouple, which terminated beyond the low-$\bar{g}$ interval of solidification.

The thermal profiles of each sample solidified in low-$\bar{g}$ are quite similar to those observed in the 1-$\bar{g}$ comparision experiment. This is shown in Fig. 19 for samples solidified in furnace assembly No. 1; the temperature profile as a function of distance from the solidification interface, as well as the thermal gradients near the solidification interface, are statistically equivalent for all samples, as is shown in Table 1. This distance from the solidification interface was deduced from the time of solidification and furnace velocity, assuming that the location of the interface coincides with the discontinuity in the thermal profile.

Magnetic Properties

The magnetic properties of both the low-$\bar{g}$ flight and 1-$\bar{g}$ All-Systems Test samples were also very similar in that both were dominated by the HC (high coercivity) phase. As shown in Fig. 20 for samples grown in furnace assembly No. 1, the first quadrant demagnetization curves at room temperature (samples first exposed to an applied magnetic field of 150 kOe) indicate a remanent magnetization of 0.1 emu/g of Bi/MnBi. The remanent magnetization data suggest that both the low-$\bar{g}$ and 1-$\bar{g}$ samples contain > 95 v/o HC phase. By deconvoluting the magnetization into HC phase and LTP phase components (Ref 9-12) and normalizing to equivalent v/o of dispersed MnBi using correlations established during ground base experiments, we found that the low-$\bar{g}$ samples contained 7 ± 1% less v/o MnBi than the 1-$\bar{g}$ samples as seen in Table 1. The mean 1-$\bar{g}$ value of 3.18 v/o MnBi corresponds to the anticipated nominal value determined for eutectic Bi/MnBi (Ref 7).

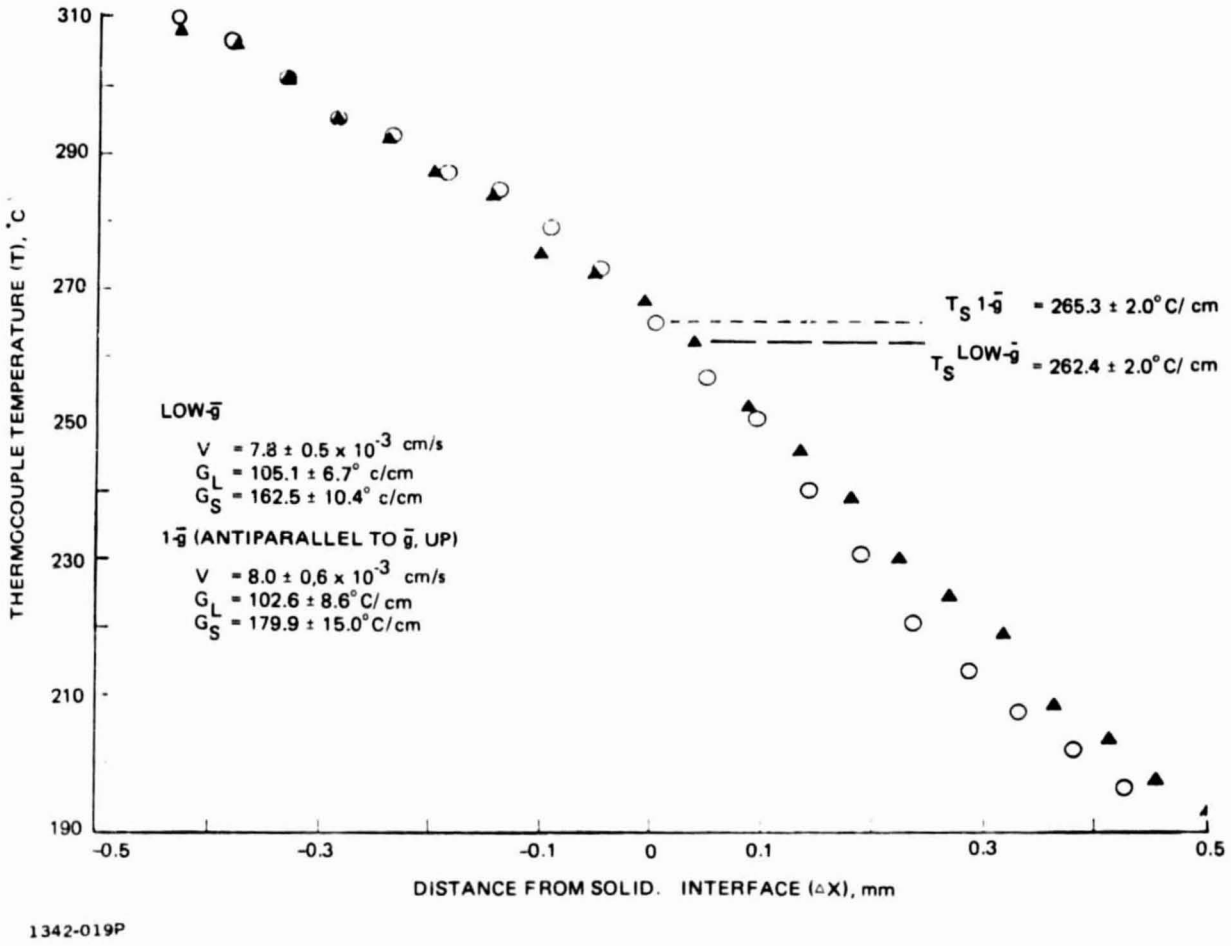

Fig. 19 Comparison of Flight and All Systems Test Thermal Profiles Near Solidification Temperature for Samples Solidified in Furnace Assembly No. 1

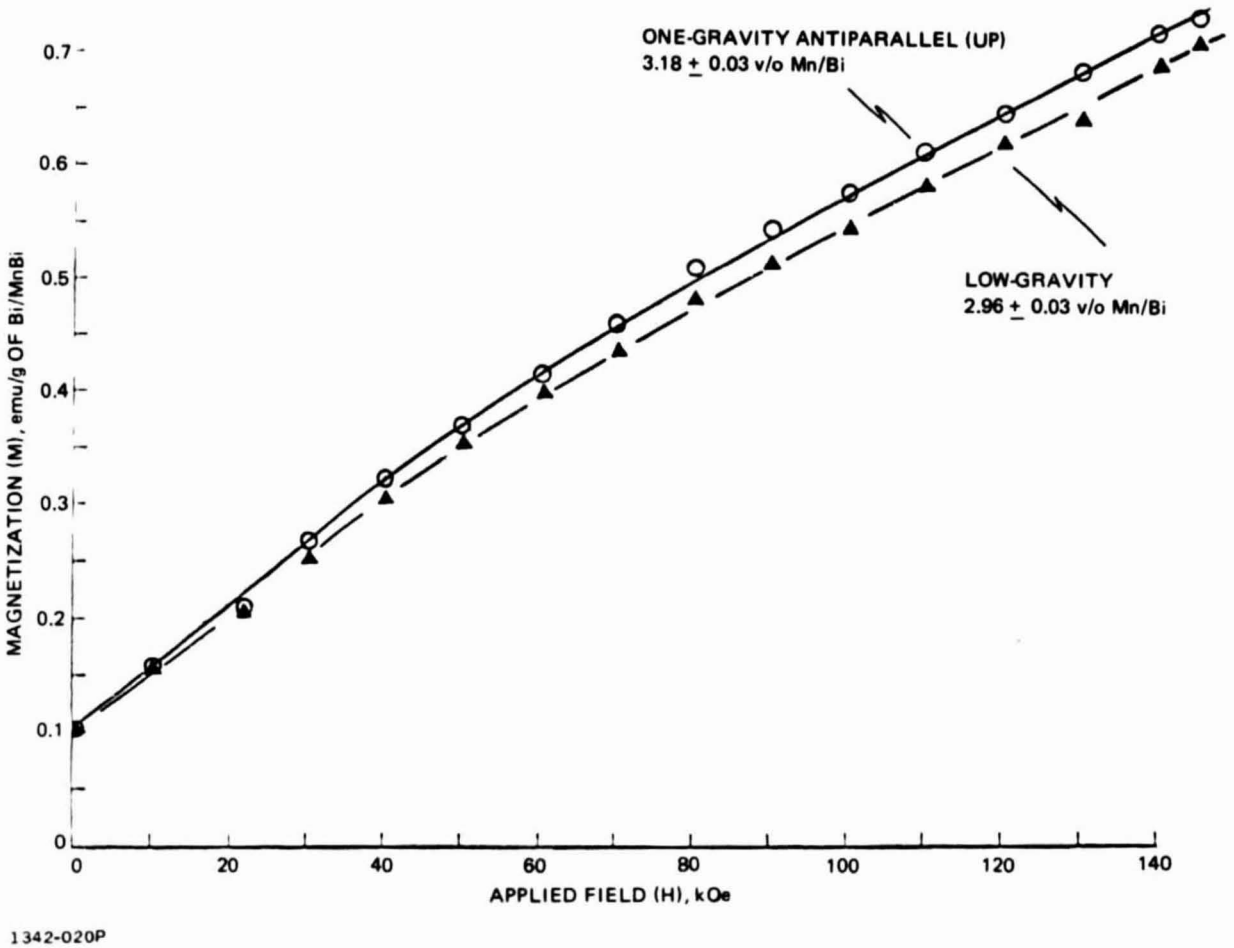

1342-020P

Fig. 20 First Quadrant Demagnetization of Flight vs All Systems Test Samples Solidified During Low-$\bar{g}$ Interval in Furnace Assembly No. 1 Indicating Lower v/o Dispersed MnBi for Low-$\bar{g}$ Sample

In addition, selected flight and ground base comparison samples were isothermally heat treated and their room temperature hysteresis measured after each anneal cycle. Identical fraction solidified segments, corresponding to the low-$\bar{g}$ interval of solidification, were heat treated together in the same apparatus and allowed to cool slowly from the anneal temperature of 220°C. The v/o of dispersed MnBi of both low-$\bar{g}$ and 1-$\bar{g}$ samples remains essentially unchanged from the as-grown state while the intrinsic coercivity of the low-$\bar{g}$ samples, as seen in Fig. 21, is consistently larger with respect to the 1-$\bar{g}$ comparison sample. Also shown in Fig. 21 is a similar study of samples grown in the PIAT test. The higher intrinsic coercivity obtained from the same time at temperature anneal in the low-$\bar{g}$ samples supports the smaller particle size or rod diameter distributions observed in the morphology studies.

A set of postflight samples were also grown in the SPAR VI flight apparatus at General Electric/Valley Forge under PIAT conditions. Those samples were identical in morphology, thermal, and magnetic properties with respect to the preflight All-Systems Test samples, indicating that no anomalies had occurred in the ADSS apparatus as a result of the launch or flight experiment.

Laboratory (1-$\bar{g}$) Experiments - Morphology & Thermal Properties

In the high furnace rate regime of V $\sim$30 cm/h, comparable to the SPAR VI flight, samples were grown up, down, and horizontal to the gravity field in an effort to change the degree of thermal and solutal convection present. However, as pointed out by Coriell (Ref 14), the interaction of the solute and temperature gradients is complex and a priori effects are difficult to estimate. For example, a statically unstable density profile (growth down) without convection, as well as a statically stable density profile (growth up) with convection, can occur.

The first observation is that, regardless of growth orientation, at V $\sim$30 cm/h and G_L $\sim$100°C/cm, there exists significant nonhomogeniety, on a small microscopic scale, in the measured volume fraction of MnBi from region to region, even at the same fraction solidified. The size of each areal region measured was typically $\sim$2500 μm^2 with an average population of 375 $\pm$ 50 particles. This inhomogeniety is shown in Fig. 22 for samples grown up and down during the All-Systems Test. If a suitable number of regions were considered or, conversely, one large-enough region monitored, the variance in bulk volume fraction was small ($\pm$5% v/o MnBi) compared with a variance in volume fraction as large as $\pm$ 25% for

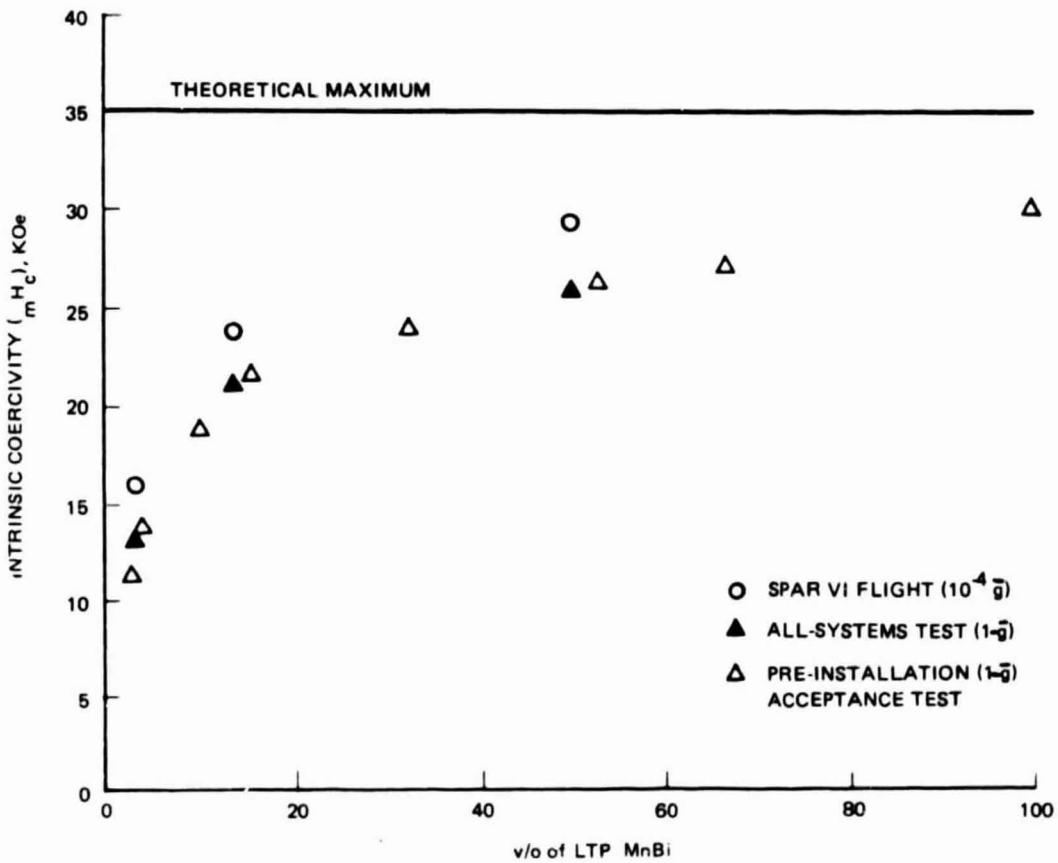

1342-021P

Fig. 21 Effect of Isothermal Annealing of PIAT (Growth up to $\bar{g}$), All-Systems Test (Growth up to $\bar{g}$) and Flight Sample No. 1 on Magnetic Intrinsic Coercivity as a Function of v/o LTP MnBi Transformed. Faster rate of increase in flight sample suggests smaller rod diameter distribution for sample solidified in low $\bar{g}$.

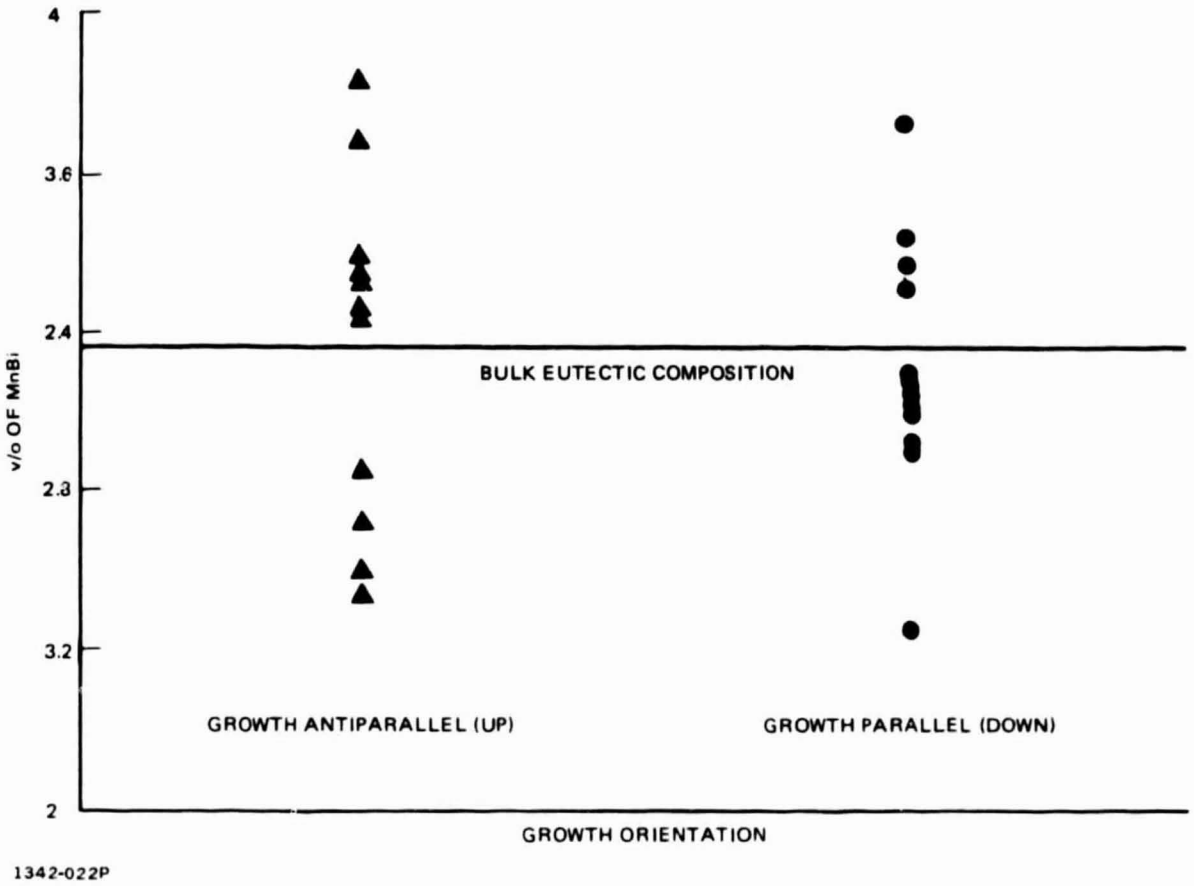

Fig. 22 Local Volume Fraction Measured by Computed-Aided Particle Analysis for Growth Up and Down at V = 30 cm/hr and G_L = 100° C/cm

each areal region. In any case, the mean volume fraction corresponded to the bulk eutectic composition of 3.18 v/o MnBi. Both the rod diameter and interrod spacing distributions were also rather insensitive to growth orientation. As is shown in Fig. 23 and 24, the shape and mean of both the rod diameter and interrod spacings are quite similar in each orientation even though growth down has a larger median and asymmetry than growth up or horizontal Statistically, the distributions are equivalent. The thermal profiles for each growth orientation were also very similar at these high furnace rate and thermal gradient conditions.

Samples were also grown at one order of magnitude lower furnace velocity ($V \sim 3$ cm/h) in both high ($G_L \sim 150°C/cm$) and low ($G_L \sim 20°C/cm$) thermal gradients. It was anticipated that, at the lower growth velocity, the solute boundary layer or Stefan length, p^{-1}, would be increased from ~ 25 μm at V = 30 cm/h to 250 μm at V = 3 cm/h where

$$p^{-1} = D_L/V \qquad (2)$$

and V is the interface or growth velocity, and D_L is the diffusion coefficient in the liquid at the eutectic composition, taken to be 2×10^{-5} cm^2/s. The calculated mass transfer film thickness, δ_m, however, assuming that a vertical flat plate-type model is appropriate (Ref 5), is expected to be on the order of 50 μm for G_L = 150°C/cm and 80 μm for G_L = 20°C/cm, where

$$\delta_m = (Pr/2.41\ Sc)^{1/3}\ L \left\{(1 + [0.95/Pr])/Pr(\bar{g}\,\alpha\,\Delta T L^3/\gamma^2)\right\}^{1/4}$$

and Pr = Prandtl number

Sc = Schmidt number

L = characteristic length or diameter of the ampoule

$\bar{g}$ = magnitude of the gravitational force

α = percent change in liquid density with temperature

ΔT = temperature difference in the system

γ = kinematic v scosity.

Notice that δ_m is not a function of V and varies with $\bar{g}^{1/4}$. For G_L = 150°C/cm, the ratio δ_m/p^{-1} or $p\,\delta_m$ would be expected to vary from 2 at V = 30 cm/h to 0.2 at V = 3 cm/h and we would, therefore, expect convection to have a greater influence at the lower growth velocity since convection should become increasingly more important as a mass transport mechanism as $p\,\delta_m \longrightarrow 0$ while diffusion dominates for $p\,\delta_m >> 1$.

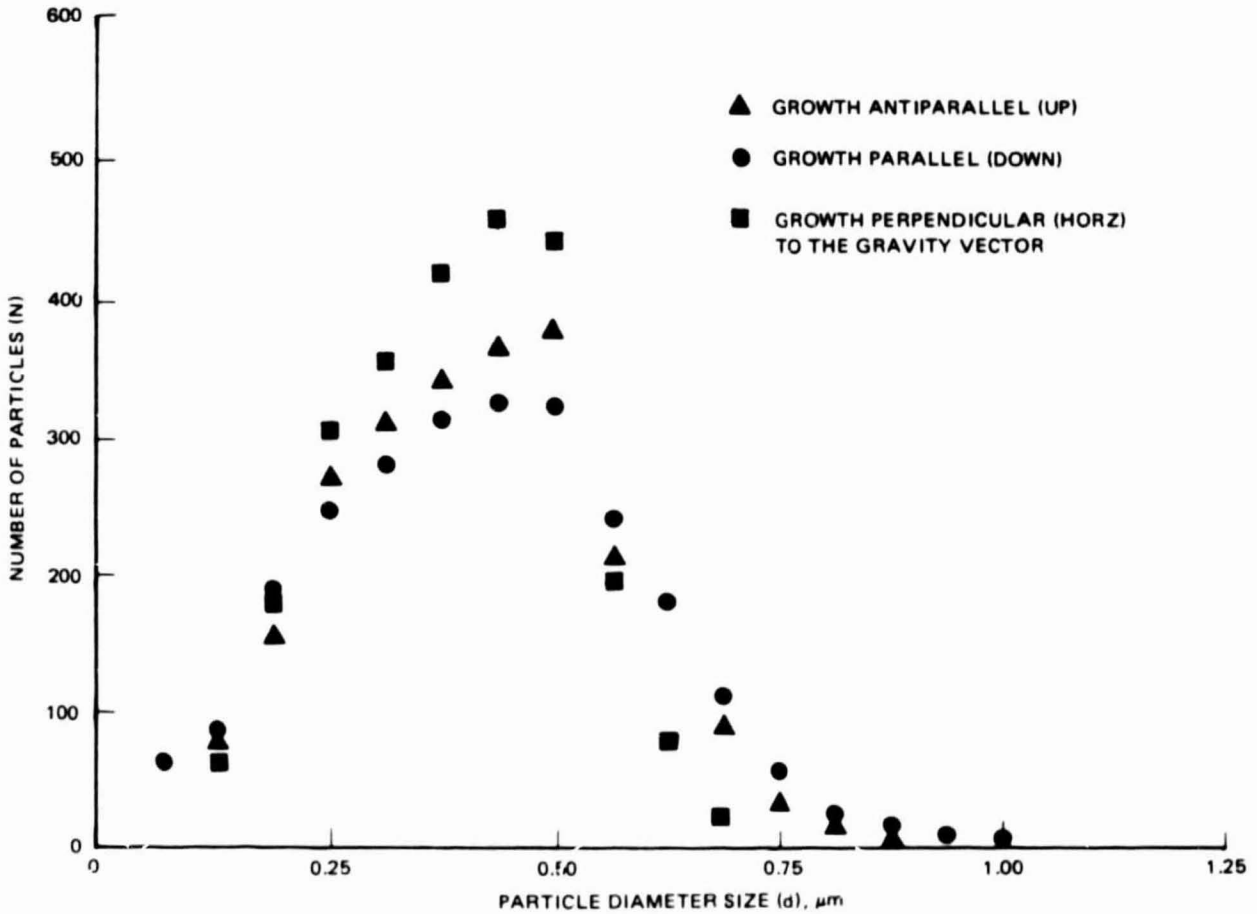

Fig. 23 Dispersed MnBi Rod Diameter Distributions as a Function of Solidification Orientation Axis in 1-$\vec{g}$ at V=30 cm/hr and $G_L = 100^{\circ}$ C/cm

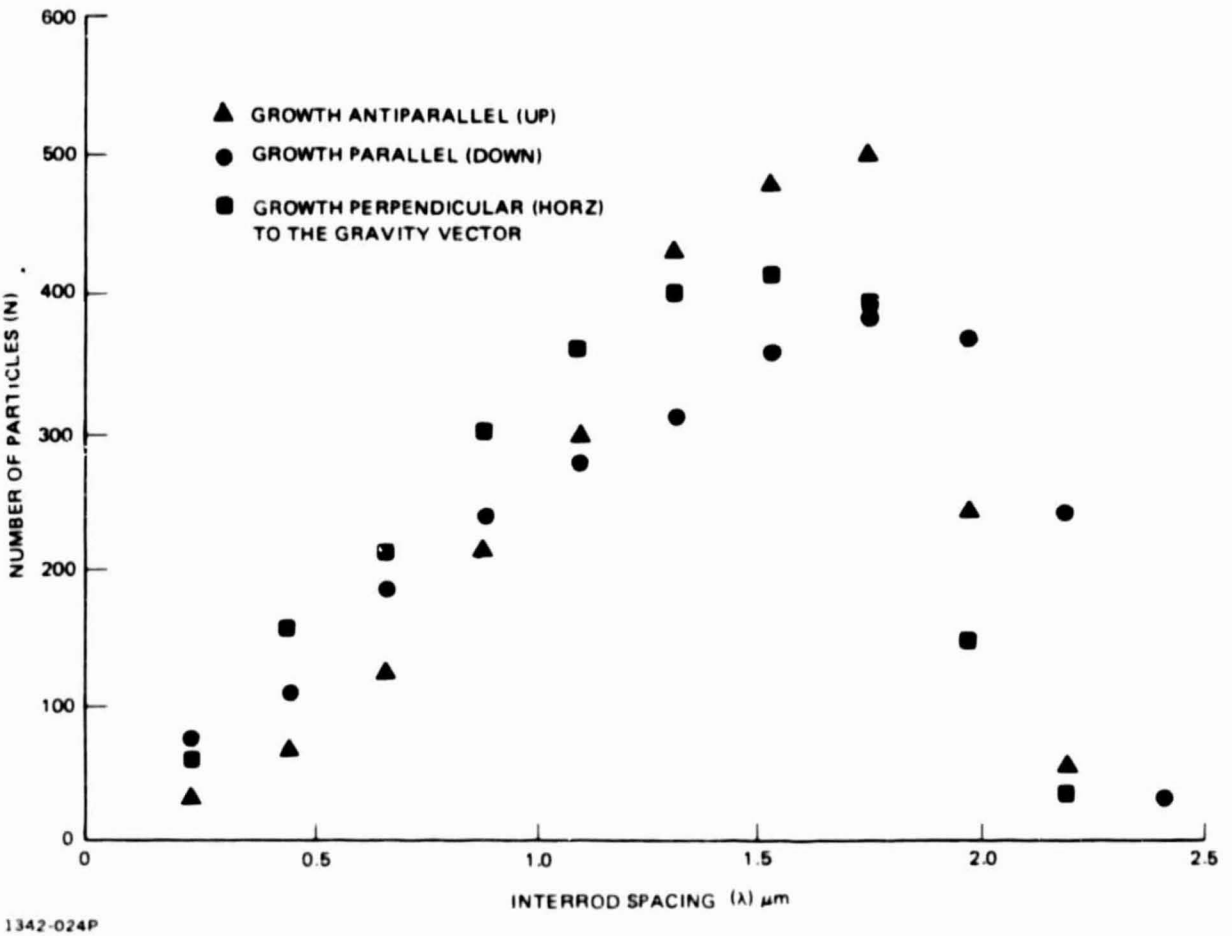

Fig. 24 Interrod Distributions of Dispersed MnBi Rods Measured Transverse to Solidification Direction as a Function of Growth Orientation at V=3 0 cm/h and G_L = 100° C/cm

The morphology of the lower growth velocity samples, however, also showed no dependence on growth orientation with respect to the gravity vector. As is shown in Fig. 25, the interrod spacing distributions are statistically equivalent for growth up, down, and horizontal. In addition, no change in either rod diameter or interparticle spacing (Fig. 26) was noted on decreasing the thermal gradient in the liquid by nearly an order of magnitude ($G_L \sim 150°$ to 20°C/cm). Similar studies on directionally solidified eutectic Bi/MnBi grown in larger diameter (0.7 cm inner diameter) quartz ampoules (Ref 15) have also shown no dependence of interrod spacing on thermal gradient. In addition, the inhomogeniety in local volume fraction was noted as well for $V \sim 3$ cm/h (Fig. 27).

In situ thermal measurements as a function of solidification time for $V \sim 3$ cm/h and $G_L \sim 20°C/cm$ for growth up, down, and horizontal orientations were also investigated. A typical temperature vs time profile for a growth up orientation is shown in Fig. 28. The discontinuous change in slope or thermal gradient observed in the thermogram occurs at the solidification or eutectic melting temperature and is the result of a discontinuous change in thermal conductivities between liquid ($K_L = 0.12$ $Wcm^{-1}K^{-1}$) and solid ($K_s = 0.06$ $Wcm^{-1}K^{-1}$) Bi/MnBi. The thermal gradients were deduced from the thermocouple thermograms by calculating the instantaneous slope for each temperature interval and averaging in a stepwise fashion over six consecutive measurements. The effect of varying the growth orientation on the resultant gradients with respect to the position of the solidification interface is displayed in Fig. 29. The experiment was conducted so as to maintain a similar gradient in the liquid near the solidification interface, regardless of orientation, by adjusting the temperature of the hot zone of the furnace. Hence, any effect of orientation of $\bar{g}$ would occur in the observed gradient of the solid. In fact, such an effect is observed with a steeper gradient for growth down (thermally unstable) compared with growth up (thermally stable).

Laboratory (One-Gravity) Experiments - Magnetic Properties

The volume percent of HC phase formed (normalized to v/o of dispersed MnBi) is a sensitive function of solidification processing conditions. By varying the furnace velocity over approximately two orders of magnitude, the amount of HC varies from ~10 to ~100 v/o as shown in Fig. 30. The amount of HC phase also

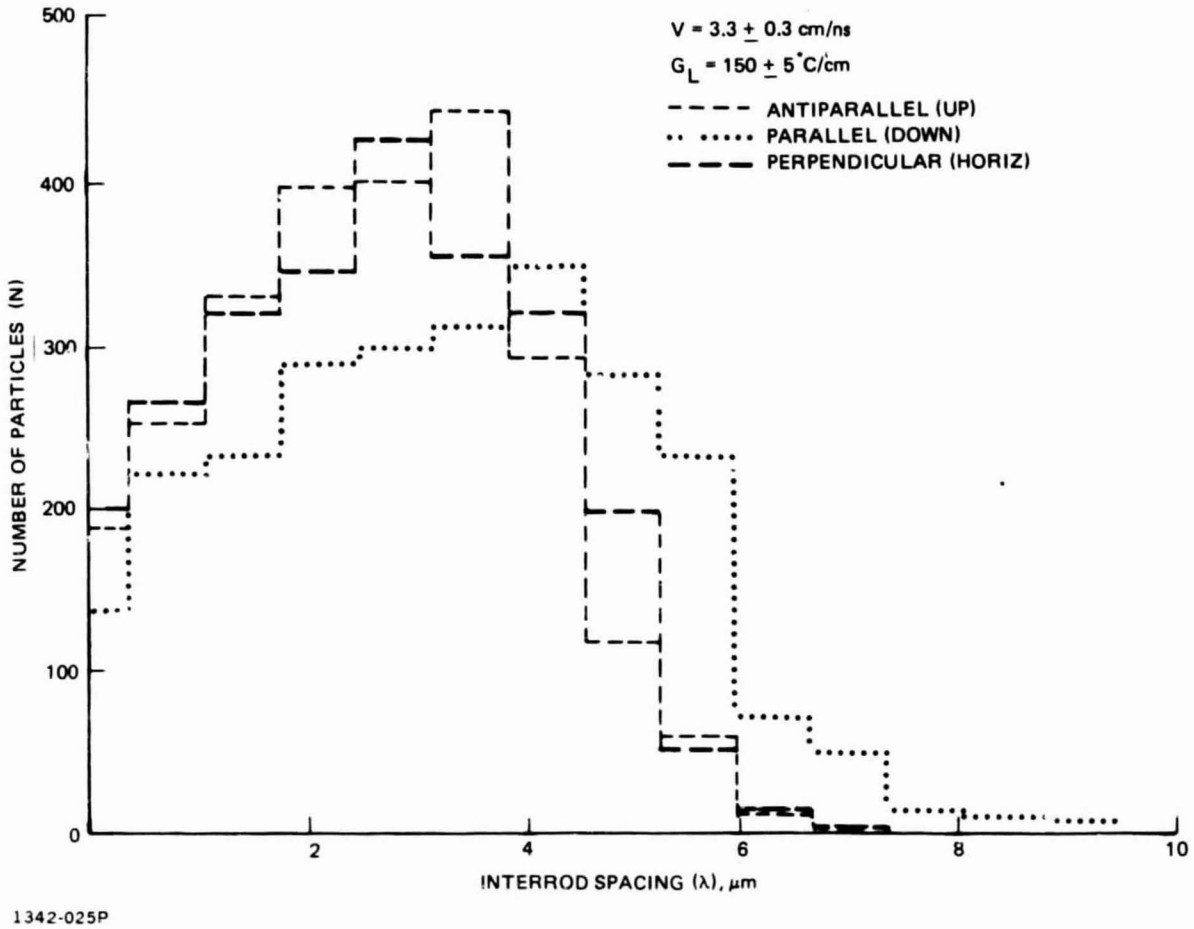

Fig. 25 Interrod Spacing Distributions as a Function of Solidification Direction in 1-$\bar{g}$ at V=3 cm/h, G_L = 150° C/cm

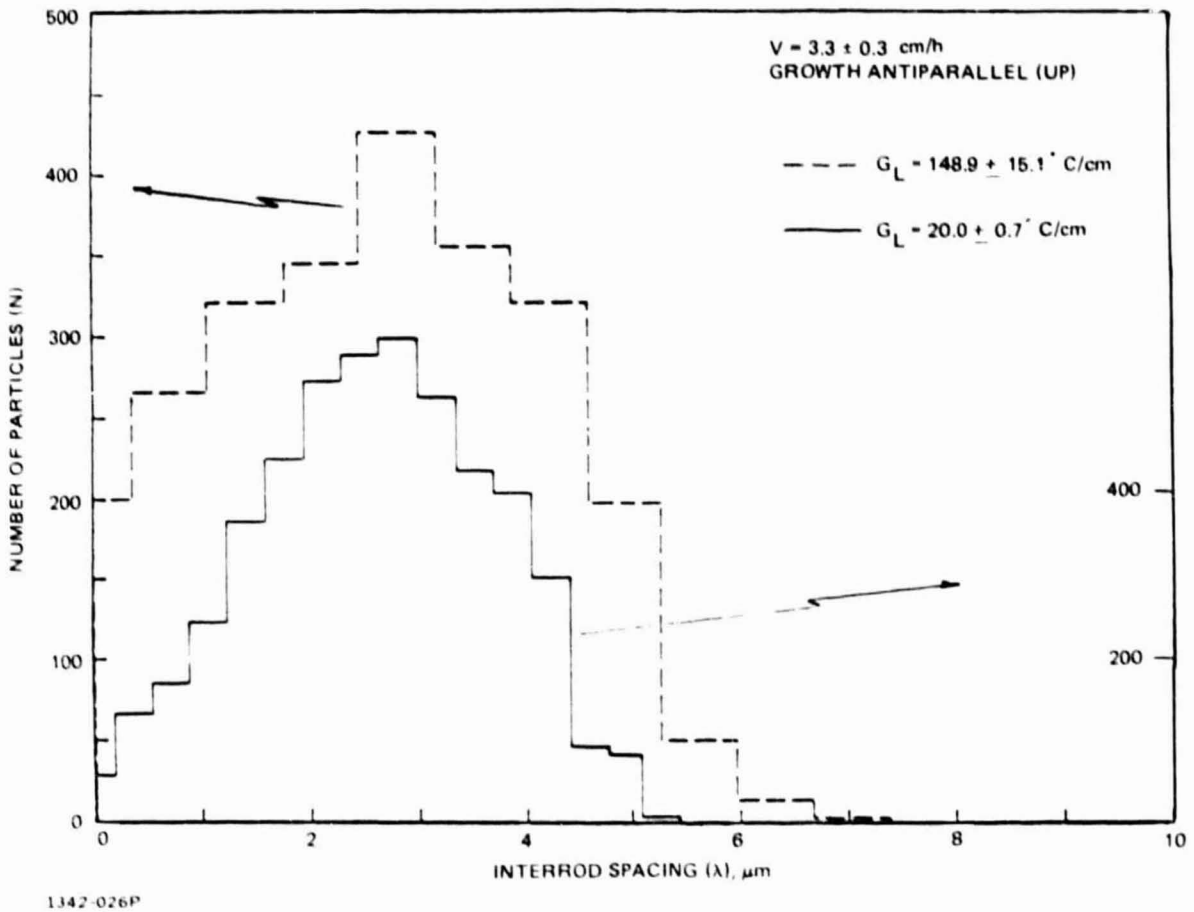

Fig. 26 Interrod Distribution Growth Up in $1\text{-}\bar{g}$ as a Function of Thermal Gradient in Liquid Near Solidification Interface

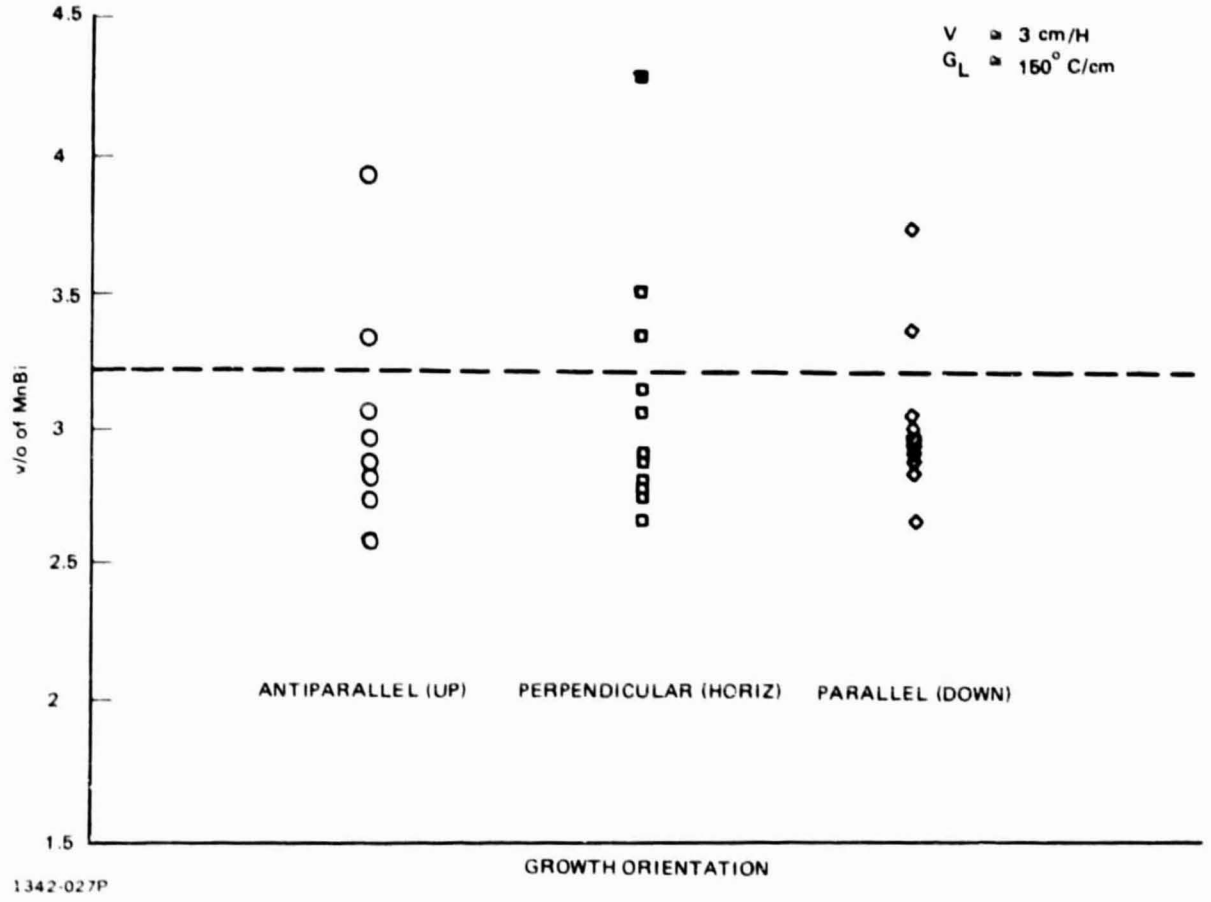

Fig. 27 Measured Local Volume Fraction as a Function of Solidification Orientation in 1-$\bar{g}$ for V=3 cm/h and G_L = 150° C/cm

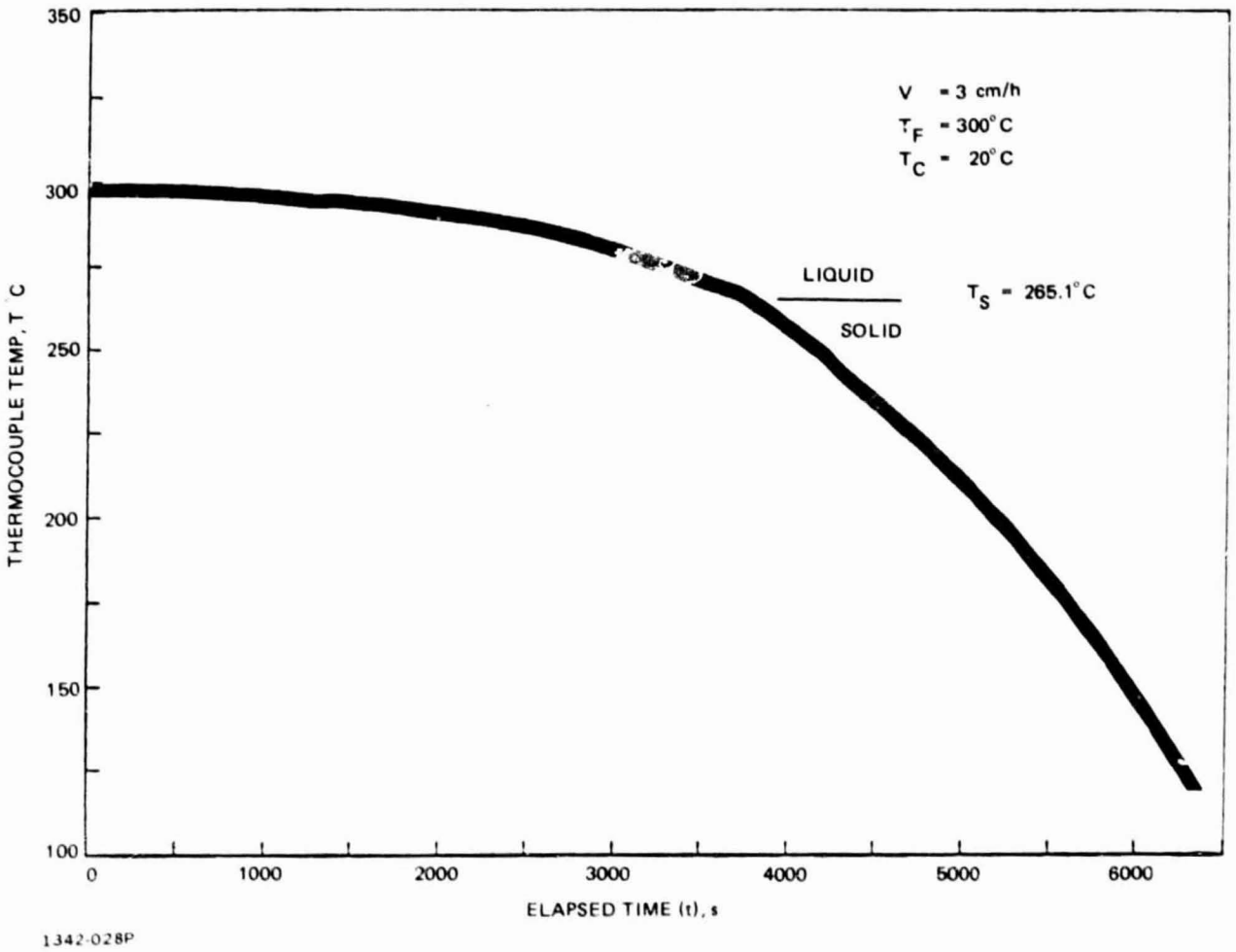

Fig. 28 In Situ Thermocouple Temperature Profile for Plane-Front Solidification of Bi/MnBi Grown Up with Respect to the Gravity Vector

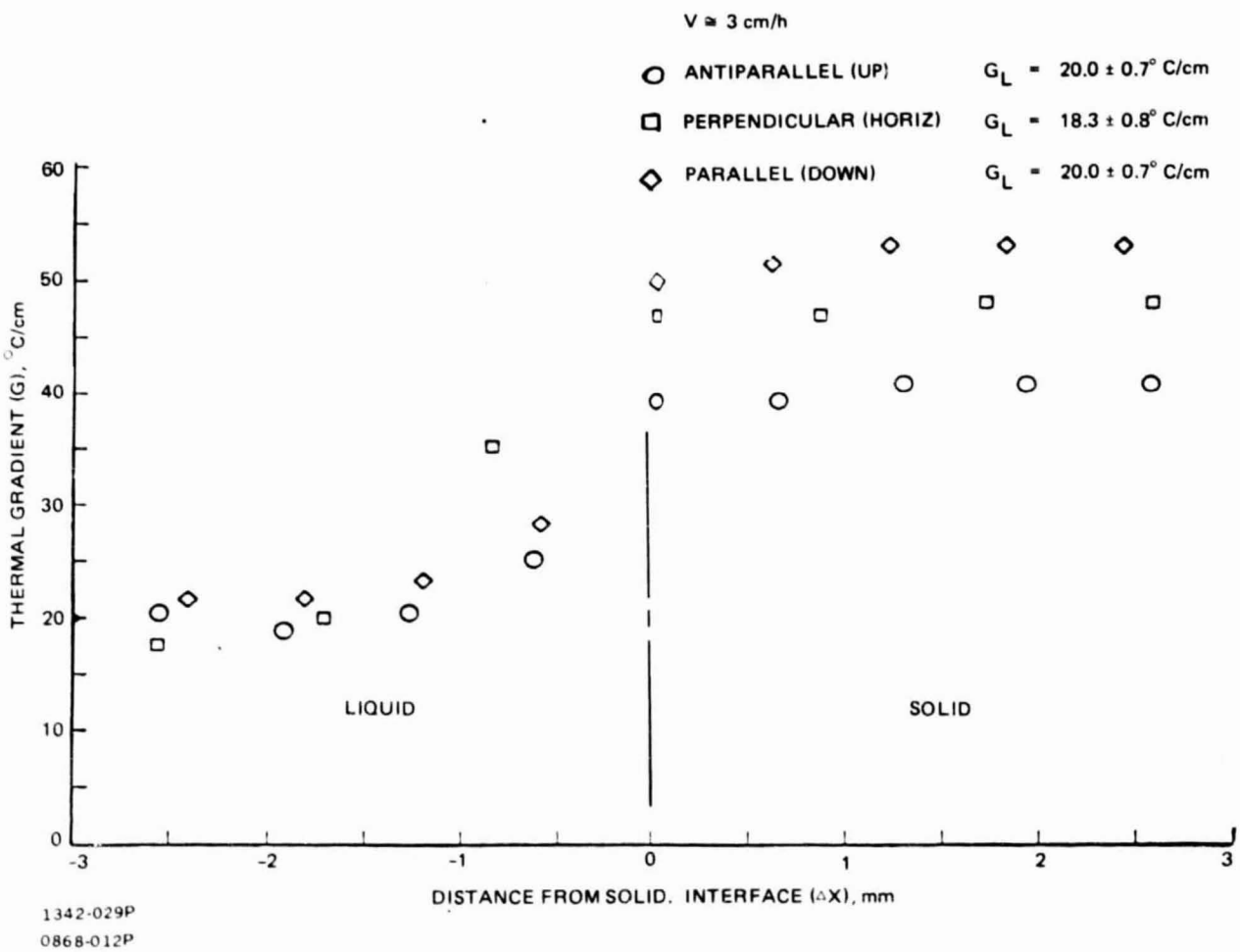

Fig. 29 In Situ Measured Thermal Gradient as a Function of Distance from Solidification Interface

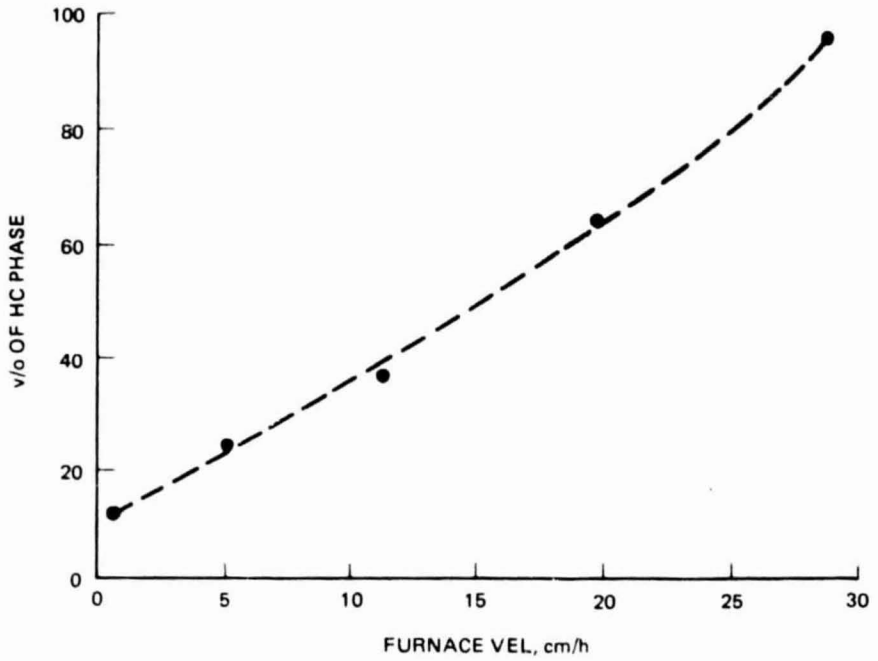

1342-030P

Fig. 30 Volume Percent of HC Phase (Normalized to Dispersed v/o MnBi) as a Function of Furnace Velocity

depends on the thermal gradient in a given growth orientation as well as the growth orientation at a given furnace velocity and thermal gradient as displayed in Fig. 31. By varying the solidification processing conditions, we have been able to isolate the magnetic behavior of the HC phase and, after appropriate heat treatment, the LTP phase in the same plane-front directionally solidified eutectic Bi/MnBi sample as seen in Fig. 32 and 33. In this way, physical observables such as the bulk v/o of dispersed MnBi can be determined from magnetization measurements.

Magnetization as a function of various angles with respect to the solidification direction was also investigated. Samples containing combinations of LTP and HC phases, as well as those containing only the LTP phase, were studied. The expected anisotropy in intrinsic coercivity was observed in all samples suggesting that the c-axis of the hexagonal NiAs structure of LTP MnBi (easy axis of magnetization) lies parallel to the solidification direction regardless of the amount of HC phase present. By monitoring the remanent magnetization as a function of angle with respect to the solidification direction, the degree of alignment of the MnBi rods can be determined since the remanent magnetization is maximum parallel to the solidification direction (long axis of the rods) and zero perpendicular, and should, theoretically, follow a cos θ behavior for an ideal alignment. Figure 34 shows that the All-Systems Test samples were almost perfectly aligned with a variance of $\pm 2°$. In addition, the magnetic properties of the All-Systems Test ($1\text{-}\bar{g}$ comparison to SPAR IV flight samples) samples indicated that they contained >95 v/o HC phase regardless of growth orientation at $V \sim 30$ cm/h and $G_L \sim 100°C/cm$.

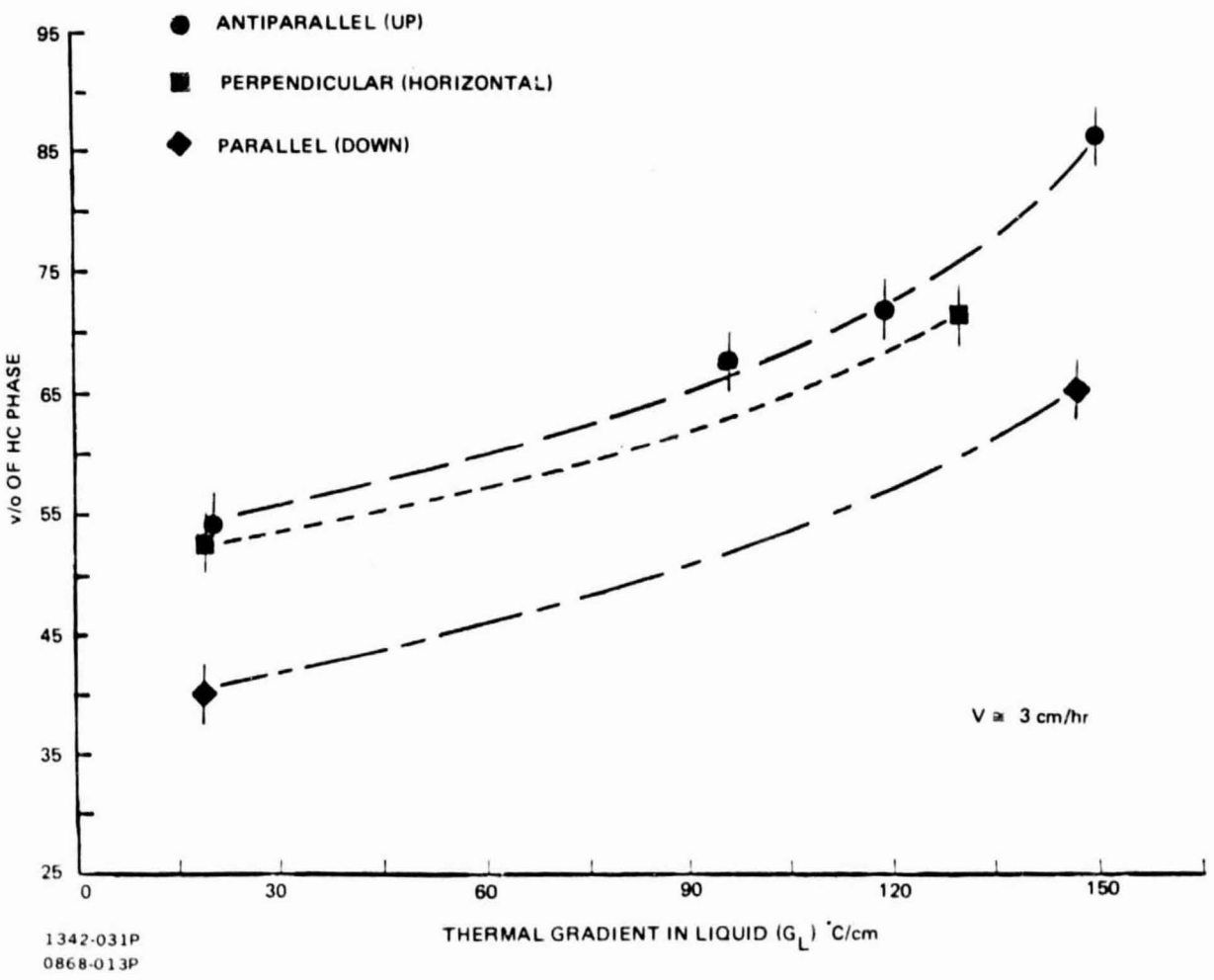

Fig. 31 Effect of Thermal Gradient and Gravity Vector Orientation During Solidification on Formation of HC Phase

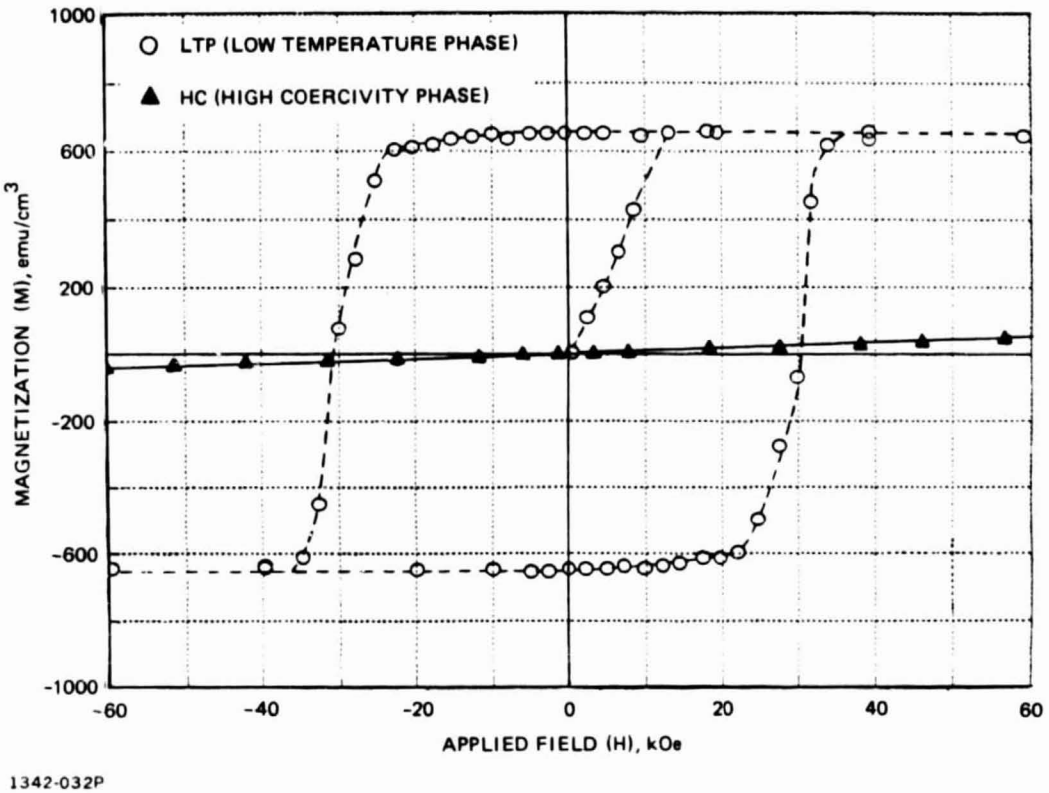

Fig. 32 Magnetization per Unit Volume of Dispersed MnBi at 290 K Parallel to Solidification Direction for a Sample with Average Rod Diameter $< d > = 0.4\ \mu m$ in the As-Grown State (▲) Containing >99 v/o HC Phase and Fully Annealed (o) Containing only LTP Phase

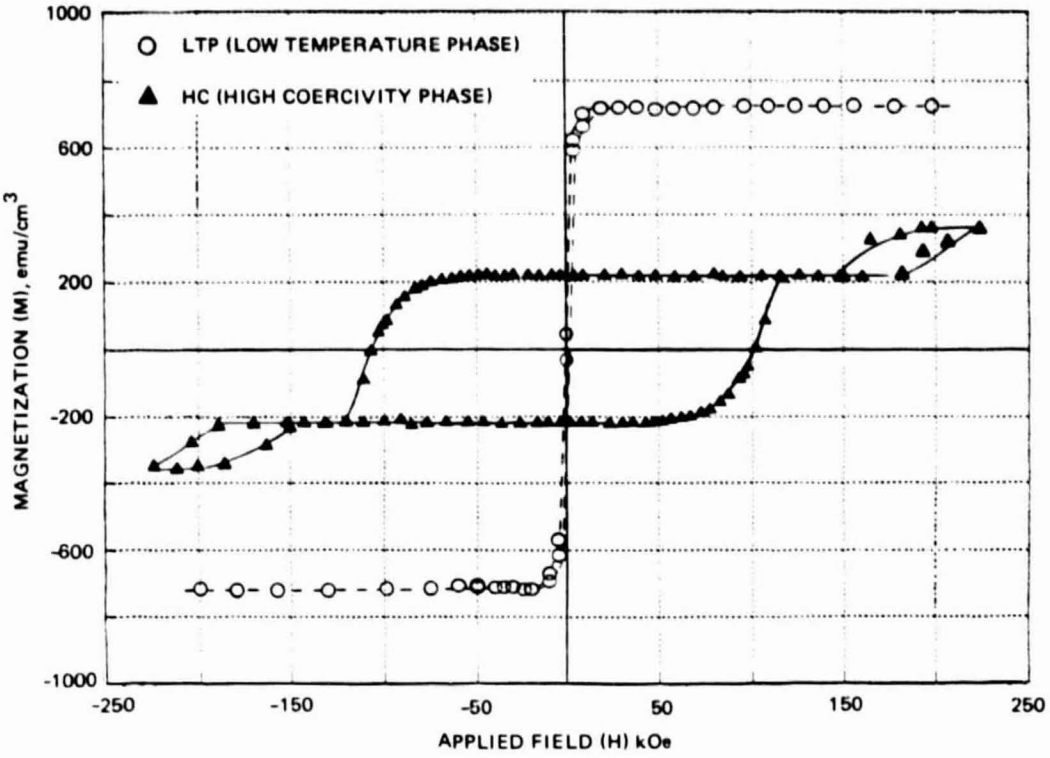

1342-033P

Fig. 33 Hystersis Curve at 77 K Parallel to Solidification Direction for Sample Displayed in Fig. 32

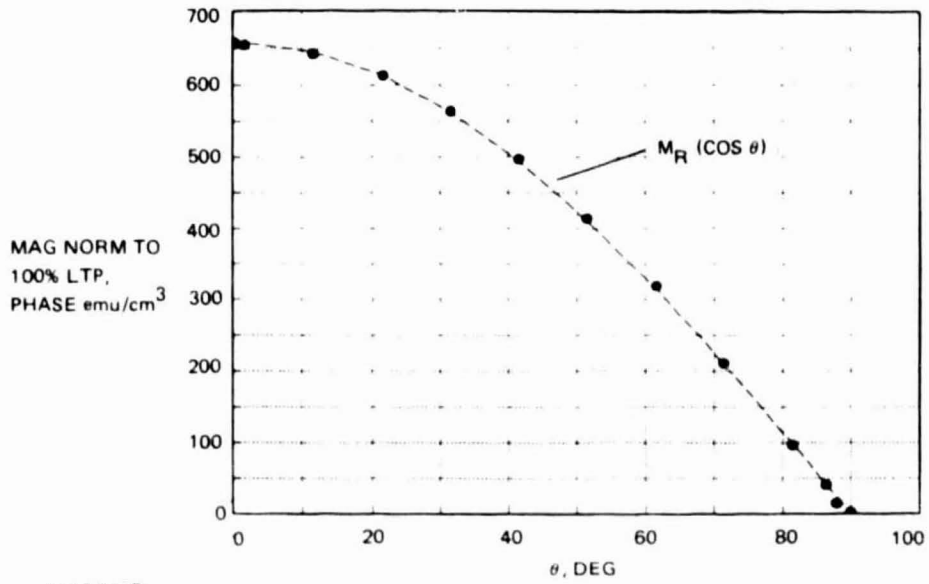

1342-034P
1997-024B

Fig. 34 Remanent Magnetization as a Function of Solidification Direction of LTP MnBi Component for Sample Containing Both LTP and HC Phases

DISCUSSION

CANDIDATE MECHANISM - Low-$\bar{g}$ vs 1-$\bar{g}$ DIFFERENCES

It has been observed that one effect of thermal convection, in plane-front solidification processing, is to introduce temperature fluctuations in the melt when the temperature gradient exceeds a critical value that depends on intrinsic properties of the particular system being solidified (Ref 16-21). Specifically, when the ratio of buoyancy forces to viscous forces in the liquid (Rayleigh number, N_{RA}) exceeds a critical value, regular or oscillatory temperature fluctuations may occur. At very high values of N_{RA}, these fluctuations may become irregular and are thought to represent turbulent flow.

When these temperature fluctuations reach the liquid-solid interface, they may induce nonsteady-state interface motion. For oscillatory fluctuations, the interface would periodically decelerate before moving forward again. Such oscillatory or irregular interface movement would increase as the fluctuations increase (higher thermal gradient). One result of the unsteady interface motion for growth of a rod eutectic might be to decrease the mean interface or growth velocity assuming that insufficient time was available for the rod spacing to adjust to an increasing growth velocity during the period of oscillation by, for example, a branching-type mechanism. As the gravitational force is decreased and the buoyancy forces are reduced (smaller Grashof number, N_{GR}), the amplitude of oscillations would decrease until the interface motion achieved steady state (low-$\bar{g}$), resulting in a higher mean growth velocity that should approach the furnace velocity.

As a result of an increase of mean growth velocity moving from 1-$\bar{g}$ to low-$\bar{g}$, one would expect the relation between rod spacing, λ, total interface undercooling, ΔT and growth or interface velocity, V, to reflect this difference. As is shown in Fig. 35, a schematic illustration of the Hunt and Jackson type function (Ref 22), relating interfacial undercooling to mean growth velocity,

$$\Delta T = AV\lambda + B/\lambda \qquad (4)$$

where A and B are constants that depend on the particular alloy system, suggests that an increase in V (V to 2V) could result in a simultaneous decrease in λ and increase in ΔT. One effect of a change in undercooling would be to alter the

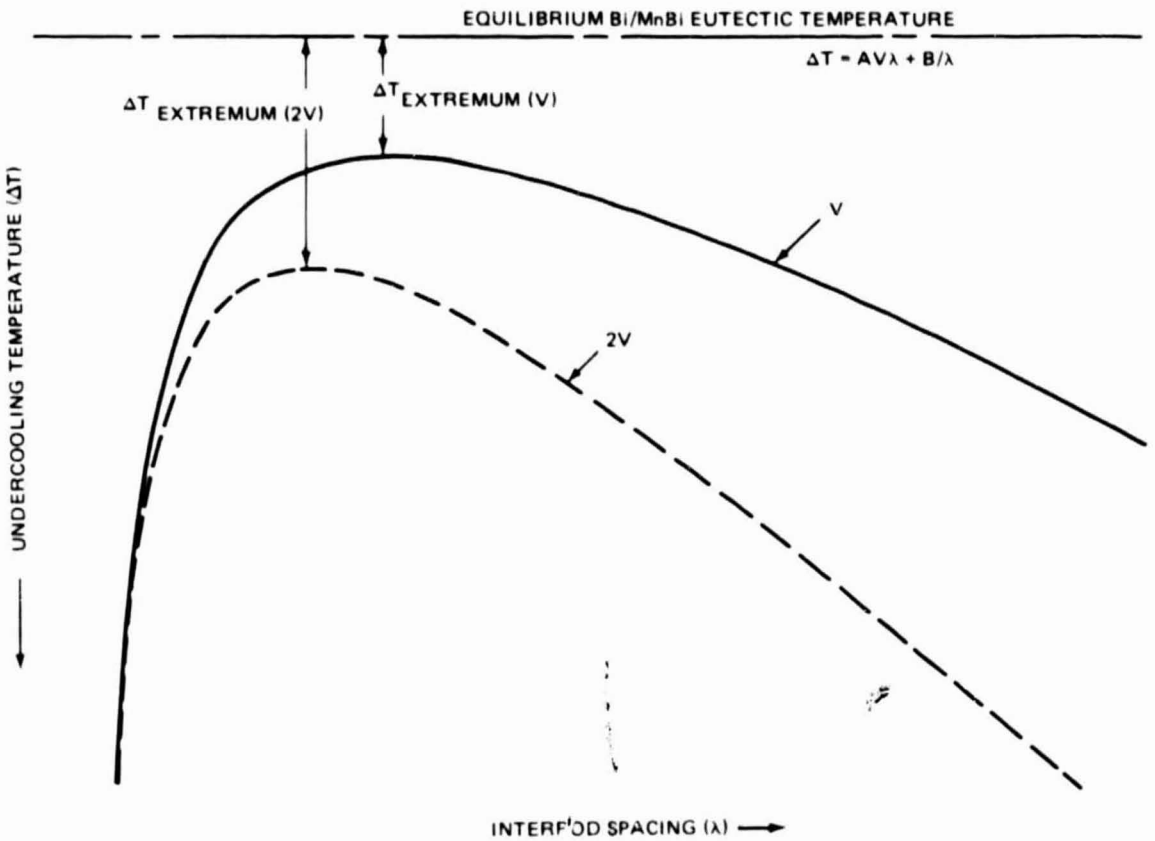

Fig. 35 Hunt-Jackson Relation Among Undercooling of Eutectic Melting Point, Growth Velocity, and Mean Interrod Spacing

phase diagram in the vicinity of the eutectic as shown in Fig. 36. The limit of solid solubility would be increased as would the eutectic composition. However, since Bi/MnBi is a rather low volume fraction eutectic with asymmetrical liquidus slopes near the eutectic composition, a decrease would be anticipated in both weight fraction MnBi (assuming the stoichiometry of MnBi remains at 50 a/o) as well as volume fraction of dispersed MnBi. In fact, such a decrease in MnBi volume fraction was observed in our low-$\bar{g}$ solidified samples.

There are, of course, other explanations that may be responsible for the observed differences between 1-$\bar{g}$ and low-$\bar{g}$. These include the influence of convectively driven fluid flow or the magnitude of the gravitional force on heat and mass transport coefficients and interfacial energies leading to different boundary growth conditions in 1-$\bar{g}$ and low-$\bar{g}$.

1-$\bar{g}$ EFFECTS

The lack of sensitivity of morphology to various levels of convection for samples grown in 1-$\bar{g}$ may indicate that, for boundary layer thicknesses equal to or larger than interrod spacings ($\delta_m \geq \lambda$), the presence of convection has little direct effect on the spacing or rod diameter distributions (Ref 23) of eutectic Bi/MnBi. Even at the lower growth velocities investigated, V = 3.0 cm/h, $\lambda \sim 3$ μm, which is much smaller than the predicted $\delta_m \sim 50$ μm, suggesting that the eutectic is tightly coupled. At this lower growth velocity, however, $p\delta_m \sim 0.2$, which would be expected to lead to, for example, severe convectively-driven macrosegregation for plane-front directionally solidified off-eutectic Bi/MnBi, indicative of a strong convective influence. In fact, such macrosegregation has been observed for Bi-rich off-eutectic Bi/MnBi bulk starting compositions (Ref 24). The variation in observed thermal gradients for eutectic Bi/MnBi grown at V$\sim$ 3 cm/h and $G_L \sim 20°C/cm$ ($p\delta_m \sim 0.3$), as a function of growth orientation with respect to $\bar{g}$, also shows a convective effective. Lastly, the amount of metastable magnetic MnBi phase produced in directionally solidified Bi/MnBi varies strongly with growth orientation in 1-$\bar{g}$. The origin of this dependence may be due to the different cooling rates (anneal time at temperature) experienced in different growth orientations or may be indicative of the convective flows or thermal instabilities present at the liquid-solid interface during solidification in 1 $\bar{g}$.

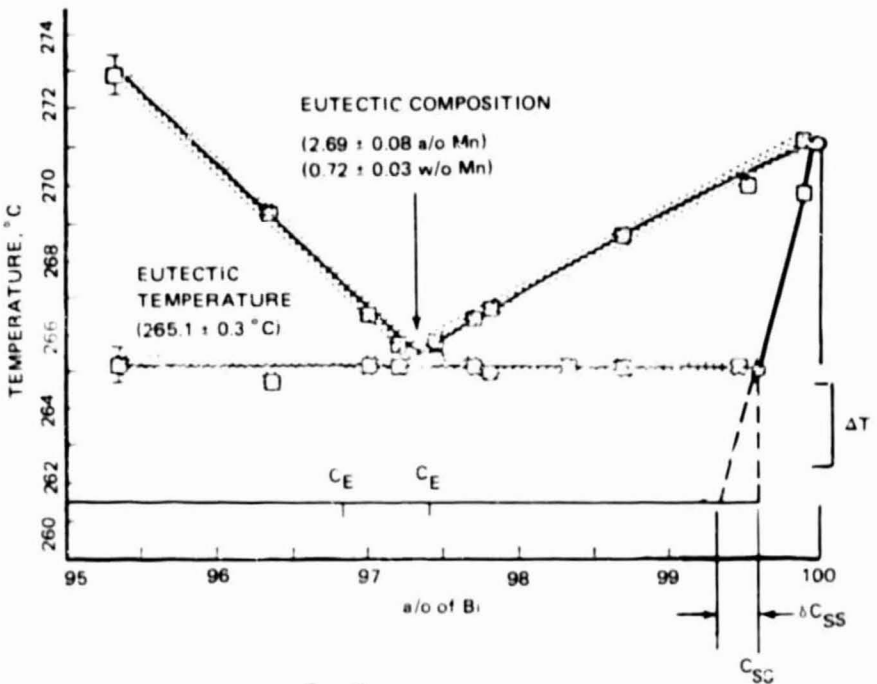

$$\text{WEIGHT FRACTION MnBi} = \frac{C_E - C_{SS}}{C_{MnBi} - C_{SS}} = F$$

$$\frac{\delta F}{F} = \frac{\delta C_{SS}}{C_E - C_{SS}} \cdot \frac{C_{MnBi} - C_E}{C_{MnBi} - C_{SS}}$$

FOR $\Delta T \sim 3^\circ C$, $\delta F/F \sim 7\%$

1342-036P

Fig. 36 Effect of Interfacial Undercooling on Equilibrium Diagram and Weight Fraction MnBi in Vicinity of Eutectic

PRINCIPLE OF PHYSICAL SIMILARITY

It has been recently noted (Ref 25) that additional insight as to the influence of gravity on crystal growth may be obtained by applying the principles of physical similarity to the specific system under investigation on earth and in the microgravity of space. It is necessary to identify a complete set of physical observables that characterize physical phenomena that occur in each system, i.e., 1-$\bar{g}$ of earth and low-$\bar{g}$ of space. It is usually chosen to select dimensionless groups that contain the gravitational force, $\bar{g}$. The corresponding dimensionless groups may be chosen to be $\bar{g}$ divided by some other characteristic acceleration; for example, in the case of thermally driven convection, this characteristic acceleration may be taken to be

$$a_{char} = \gamma^2/(\alpha \Delta T\, L^3) \qquad (5)$$

where γ is the kinematic viscosity, α the percent change in liquid density with temperature, ΔT the temperature difference in the system, and L the charcteristic length. The resulting dimensionless group is then the Grashof number, N_{Gr}

$$N_{Gr} = \bar{g}\,(\alpha \Delta T\, L^3/\gamma^2) \qquad (6)$$

If temperature fluctuations are responsible for a decrease in mean interface velocity, then these fluctuations should be proportional to the Grashof number through the buoyancy forces (gravitational force) and temperature difference of the system. By reducing the gravitational force, we can vary the effective interface velocity with a higher mean velocity and lower MnBi interrod and rod diameter length in low $\bar{g}$.

We have also observed, however, that the microstructure achieved in low $\bar{g}$ ($V \sim 30$ cm/h, $G_L \sim 100°C/cm$) can be duplicated in 1-$\bar{g}$ by growing at a sufficiently higher furnace velocity ($V \sim 50$ cm/h, $G_L \sim 100°C/cm$) since $\langle d \rangle$, $\langle \lambda \rangle \sim V^{-1/2}$. This behavior for interparticle spacing distributions is shown in Fig. 37. For the growth conditions used in 1-$\bar{g}$, however, the limit of the ADSS apparatus to remove heat in a unidirectional manner is near its limit. Experiments conducted $V \sim 60$ cm/h and $G_L \sim 100°C/cm$ have indicated the onset of severe interface curvature and noncooperative growth, presumably because the temperature at which solidification occurs is no longer within the adiabatic region of the

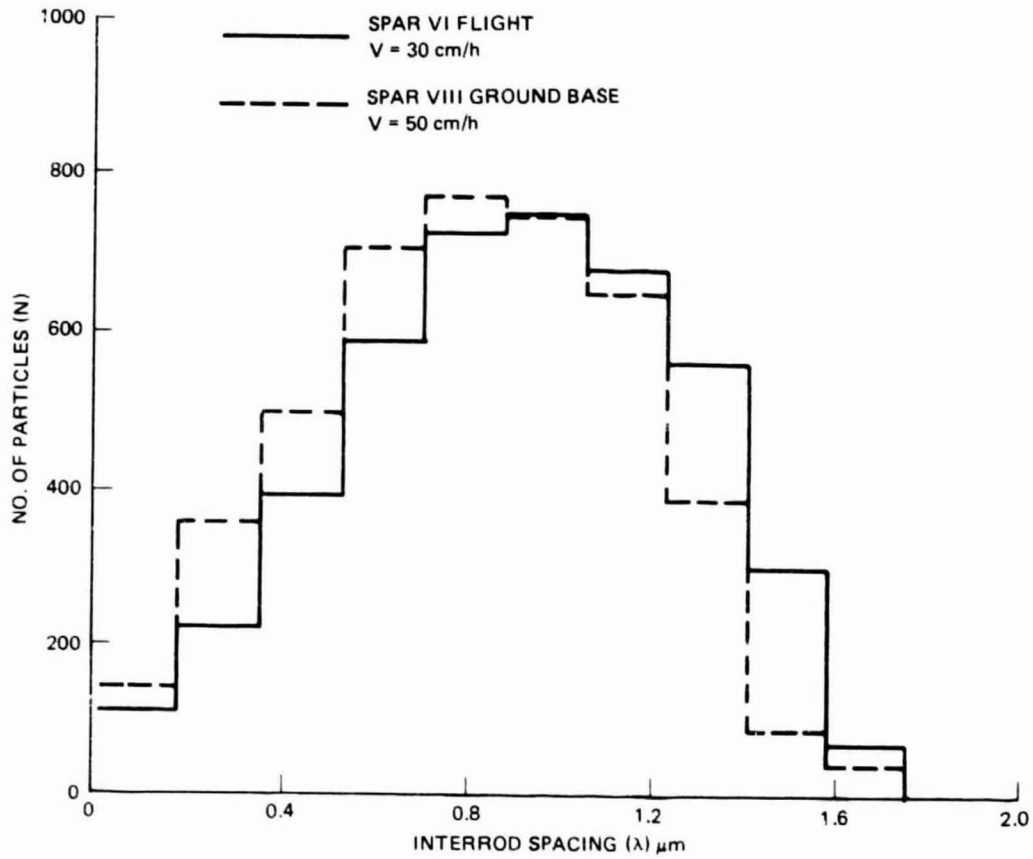

1342-037P

Fig. 37 Comparison of Measured Interrod Spacing Distributions for SPAR VI Flight Sample No. 1 (V = 30 cm/h, G_L = 100° C/cm) and Higher Growth Velocity Ground Base (1-$\bar{g}$) Sample Grown Antiparallel with Respect to Gravity Vector (V = 50 cm/h, G_L = 100° C/cm)

ADSS furnace assembly at these growth conditions. Heat transfer is thus no longer one dimensional. It may, therefore, be possible to achieve microstructures and corresponding magnetic properties for eutectic Bi/MnBi, comparable to a higher furnace velocity, in low-$\bar{g}$ that are impossible to achieve in 1-$\bar{g}$ using the same furnace assembly.

SUMMARY & FUTURE WORK

An experimental investigation of a reduced gravity environment during the SPAR VI flight and the effect of gravity vector orientation in 1-$\bar{g}$ on the plane front directional solidification of eutectic Bi/MnBi has shown:

- Statistically significant reductions in mean rod diameter, interrod spacing, and bulk volume fraction for samples solidified in low-$\bar{g}$ with respect to 1-$\bar{g}$ at V = 30 cm/h and G_L = 100°C/cm.
- No statistically significant dependence of MnBi rod diameter and interrod spacing distributions on gravity vector orientation and imposed thermal gradients during solidification over a range of V = 3 to 30 cm/h and G_L = 20 to 150°C/cm.
- That the thermal gradient in the solid depends on gravity vector orientation for V = 3 cm/h and G_L = 20°C/cm; a larger gradient was observed for the growth down direction (thermally unstable) as compared with growth up (thermally stable).
- The presence of a nonequilibrium metastable magnetic phase that coexists with the equilibirum MnBi phase and transforms during isothermal heat treatment.
- That the admixture of magnetic phases depends on growth velocity, thermal gradient, and gravity vector orientation during solidification.

A candidate mechanism involving convectively induced thermal fluctuations in 1-$\bar{g}$ is proposed to explain the differences between 1-$\bar{g}$ and SPAR VI flight results.

In view of the results obtained and candidate mechanism proposed, future experiments in both low-$\bar{g}$ and 1-$\bar{g}$ are suggested to quantify and understand the phenomena observed. Another low-$\bar{g}$ experiment should be performed at a higher growth velocity. This low-$\bar{g}$ experiment would help corroborate the present low-$\bar{g}$ results as well as provide smaller MnBi particles than we can grow in 1-$\bar{g}$. Another experiment involves utilizing applied magnetic fields and lower thermal gradients in 1-$\bar{g}$ to attempt to damp out and, therefore, minimize thermal fluctuations.

ACKNOWLEDGMENTS

The authors express their deep appreciation to G. Busch, J. Drauch, R. Lange, E. Marten, and W. Poit of Grumman for their experimental assistance and suggestions, and to P. N. Adler, W. Aubin, and J. Papazian of Grumman for technical guidance and encouragement. We would also like to thank W. Wilcox and P. S. Ravishankar of Clarkson College for their insight, experimental assistance, and guidance. We are indebted to B. Brandt, S. Foner, E. McNiff, and L. Rubin of the Francis Bitter National Magnet Laboratory for their technical assistance and rewarding discussions, as well as to M. Glicksman of Rensselaer Polytechnic Institute and C. Graham of the University of Pennsylvania for many helpful suggestions. Finally, we wish to thank R. Locker of General Electric and J. Noel and F. Reeves of the Marshall Space Flight Center for their untiring efforts in making the SPAR VI flight experiment successful.

REFERENCES

1. W. A. Tiller, "Liquid Metals and Solidification," American Society for Metals, Cleveland, Ohio, p 276, 1958.

2. J. S. Turner, Buoyancy Effects in Fluids, Cambridge, London, 1973.

3. S. R. Coriell, M. R. Cordes, W. J. Boettinger, and R. F. Sekerka, "Convective and Interfacial Instabilities During Unidirectional Solidification of a Binary Alloy, National Bureau of Standards Internal Report 78-1483, 1978.

4. W. R. Wilcox, "Effect of Freezing Rate Changes on the Mean Composition of Binary Composities," Aerospace Report No. TR-1001(2250-10)-11, El Segundo, Calif, 1967.

5. W. R. Wilcox, private communication.

6. T. Chen, "Contribution to the Equilibrium Phase Diagram of the Mn-Bi System Near MnBi," Journal of Applied Physics, Vol 45, p 2358, 1974.

7. R. G. Pirich, G. Busch, W. Poit, and D. J. Larson, Jr., "The Bi-MnBi Eutectic Region of the Bi-Mn Phase Diagram," Metallurgical Transactions A, Vol 11A, p 193, 1980.

8. General Electric Company, Space Sciences Laboratory, "Operating Manual for Automated Direction Solidification System," prepared for NASA under contract NAS8-31536, June 1978.

9. M. R. Notis, D. Shah, C. D. Graham, Jr., and S. R. Trout, "Magnetic Anisotropy in MnBi Particles Grown by Directional Solidification of the Mn-Bi Eutectic," Journal of Applied Physics, Vol 49 p 2043, 1978.

10. M. R. Notis, D. Shah, J. Young, and C. D. Graham, Jr., "Structure and Magnetic Properties of Directionally Solidified Bi-MnBi Eutectic Alloys," E Transactions, Vol MAG-15, p 957, 1979.

11. R. G. Pirich and D. J. Larson, Jr., "Magnetic and Metallurgical Properties of Directionally Solidified Bi/MnBi Composites: The Effects of Annealing," Journal of Applied Physics, Vol 50, p 2425, 1979.

12. R. G. Pirich, D. J. Larson, Jr., and G. Busch, "The Role of Processing Parameters on the Magnetic Properties of Directionally Solidified Bi/MnBi Composites," IEEE Transactions, Vol MAG-15, p 1754, 1979.

13. R. G. Pirich, "Characterization of Effects of Plane-Front Solidification and Heat Treatment On Magnetic Properties of Bi/MnBi Composites," IEEE Transactions Mag, to be published, Sept 1980.

14. W. J. Boettinger, S. R. Coriell, F. S. Biancaniello, and M. R. Cordes, "Solutal Convection During Directional Solidification," National Bureau of Standards Internal Report NBSIR 79-1767, 1979.

15. P. S. Ravishankar, Ph. D. dissertation, Clarkson College of Technology, 1979.

16., A. Muller and M. Wilhelm, "On Periodic Changes of Temperature in Liquid Crystallizing InSb," Z. Naturforsch, Vol 19a, p 254, 1964.

17. W. F. Wilcox and L. D. Fullmer, "Turbulent Free Convection in Czochralski Crystal Growth," Journal of Applied Physics, Vol 36, p 2201, 1965.

18. H. P. Utech and M. C. Flemings, "Elimination of Solute Banding in Indium Antimonide Crystals by Growth in a Magnetic Field," Journal of Applied Physics, Vol 37, p 2021, 1966.

19. H. D. Utech and M. C. Flemings, Journal of Crystal Growth, Pergamon Press, New York, p 651, 1967.

20. D. Hurle, T. J. Jakeman, and E. R. Pike, "Striated Solute Distributions Produced by Temperature Oscillations During Crystal Growth from the Melt," Journal of Crystal Growth, Vol 3/4, p 633, 1968.

21. D. Hurle, Journal of Crystal Growth, Pergamon Press, New York, p 659, 1967.

22. K. A. Jackson and J. D. Hunt, "Lamellar and Rod Eutectic Growth," Transactions of the AIME, Vol 236, p 1129, 1966.

23. J. D. Verhoeven and R. H. Homer, "The Growth of Off-Eutectic Composites from Stirred Melts," Metallurgical Transactions, Vol 1, p 3437, 1970.

24. R.G. Pirich and D. J. Larson, Jr., "The Effect of Gravity Vector Orientation during Directional Solidification on the Magnetic and Microstructural Properties of Bi/MnBi." presented at 157th Electrochemical Soc. Mtg., St. Louis, Missouri, 1980.

25. R. F. Sekerka and S. R. Coriell, "Influence of the Space Environment on Some Materials Processing Phenomena," to be published.